2011

Comparing Middle Permian and Early Triassic Environments: Mud Aggregates as a Proxy for Climate Change in the Karoo Basin, South Africa

Bryce Pludow
Colby College

COMPARING MIDDLE PERMIAN AND EARLY TRIASSIC ENVIRONMENTS: MUD AGGREGATES AS A PROXY FOR CLIMATE CHANGE IN THE KAROO BASIN, SOUTH AFRICA

B. Amelia Pludow ‘11

A Thesis

Submitted to the Faculty of the Geology Department of
Colby College in Fulfillment of the Requirements for
Honors in Geology

Waterville, Maine

May, 2011

COMPARING MIDDLE PERMIAN AND EARLY TRIASSIC ENVIRONMENTS:
MUD AGGREGATES AS A PROXY FOR CLIMATE CHANGE IN THE KAROO BASIN, SOUTH AFRICA

Except where reference is made to the work of others, the work described in this thesis is my own or was done in collaboration with my advisory committee

B. Amelia Pludow '11

Certificate of Approval:

Dr. Robert A. Gastaldo, Chair
Whipple-Coddington Professor
Department of Geology

Dr. Valerie S. Reynolds
Clare Boothe Luce Assistant Professor
Department of Geology

Dr. Bruce F. Rueger
Visiting Assistant Professor
Department of Geology

ABSTRACT

The Permian-Triassic Boundary (252.6 Ma) is an interval under intense study as changes across it represent the greatest loss of life in Earth history. Although the event is well understood and constrained in the marine realm, questions remain about extinction, climate, and environmental conditions on land. The Karoo Basin of South Africa is a focus of study due to the complete nature of its terrestrial record, specifically across this boundary.

The identification of pedogenic mud aggregates document the presence of soils with abundant clays produced in a seasonally arid environment. The occurrence of these aggregates in low-sinuosity Early Triassic fluvial samples, but not in high-sinuosity Middle Permian samples, supports the hypothesis of increasing aridity following the extinction event. Additionally, the identification of two generations of aggregates in Early Triassic channel deposits (a carbon-rich signature and a carbon-poor signature) and only one generation in paleosol deposits indicates the removal of earlier generations of paleosols from the landscape.

ACKNOWLEDGEMENTS

First and foremost, my heartfelt thanks to Dr. Robert Gastaldo for giving me the opportunity to complete this project and for all his guidance along the way. Thanks also to my thesis committee, Valerie Reynolds and Bruce Rueger for their input and feedback. To the South Africa field teams of January 2009 and 2010, I wouldn't have learned as much and it wouldn't have been nearly as much fun without you. Thanks to Marty Yates at UMO for allowing me to use their SEM and sharing his considerable knowledge. Finally, to the students of the Colby Geology Department, especially my fellow residents of Mudd 203, thanks for all the moral support during our hours spent together. This project would not have been possible without generous funding from the Dean of Faculty at Colby College.

TABLE OF CONTENTS

INTRODUCTION

The Karoo Supergroup of South Africa represents a fairly complete stratigraphic section of Upper Paleozoic and Lower Mesozoic sedimentary rock and for this reason has been studied extensively using a wide variety of tools for a multitude of purposes. In the Beaufort Group alone, spanning the Permian-Triassic, studies have focused on vertebrate biostratigraphy (e.g., Smith, 1995; Ward et al., 2000), carbon-isotope geochemistry (e.g., MacLeod et al., 2000), paleomagnetism (e.g., DeKock and Kirschvink, 2004), and whole-rock geochemical studies (e.g., Scheffler et al., 2006) to unravel paleoenvironmental conditions. However, as understanding of the Karoo Basin increases, more questions arise. Different methods of study have given rise to varying, and conflicting, hypotheses about the geological history of the basin. Additionally, studies questioning the purely aggradational nature of the Karoo sediments (e.g., Pace et al., 2009) suggest that the stratigraphic record of the basin might not be as complete as previously thought. This proposed combination of aggradational and degradational processes of terrestrial deposition further complicates the issue, making improved and additional paleoclimate proxies necessary.

This study tests hypotheses of fluvial and climate transitions between the Middle Permian and Early Triassic based on the presence of pedogenic mud aggregates in Karoo Basin deposits. Other studies focused on a variety of times and places in Earth history (e.g., Rust and Nanson, 1989; Wright and Marriott, 2007) have used the presence of aggregates in fluvial deposits as an indicator of an arid and highly seasonal climate in which Vertisols developed and were alternately wetted and dried. When eroded, sand-sized mud clasts were transported as bedload in anabranching systems, rather than as suspended load as is typical for mud-sized clasts. These aggregates can be preserved in fluvial deposits while the paleosols in which they developed have

been entirely removed from the landscape because of this transport mechanism. Thus, aggregates in fluvial channels record soil types no longer preserved in the stratigraphic record. Identifying these aggregates, whether in paleosol or channel deposits, would indicate an arid climate during the time of the features' formation based on modern analogues in Australia.

General Karoo Stratigraphy

Deposits of the Karoo Basin are presently exposed over 300,000 km^2 in South Africa and represent sedimentation beginning in the latest Carboniferous (350-300 Ma) atop older, metamorphosed rocks, and conclude with the breakup of Gondwana in the Early Jurassic (200-180 Ma). Deposition took place in environments ranging from a passive continental margin in the Paleozoic to land-locked foreland basins in the Permo-Triassic (Smith et al., 1993). The main Karoo Basin, which now extends over most of South Africa (Figure 1), was located in the southern area of Gondwana during sediment accumulation. Basin formation began with the subduction of the Paleo-Pacific plate under Gondwana which created a mountain chain, the Cape Fold Belt, and a foreland basin. The primary troughs recognized and studied within the Karoo Basin include the Karoo Trough, in the south of the basin, and the Natal Trough in the east. The Cape Supergroup was deposited into this basin, which then was deformed and metamorphosed.

As Gondwana drifted over the South Pole and continental glaciation expanded over the area, sediments of the Karoo Supergroup were deposited atop the Cape Supergroup (Johnson et al., 2006). Sedimentation began with fluvio-glacial deposits of the Dwyka Group, then continued as the resultant post-glacial epicontinental sea was infilled by deposition of the marine to deltaic Ecca Group. Initiation of fully continental deposition began with alluvial plain sediments (Beaufort Group), and grades into coarse debris fans (Molteno Formation), meander belts (Elliot Formation), arid sand dunes (Clarens Formation), and finally volcanic (Drakensberg Formation)

deposits (Figures 1 and 2). Sedimentation ceased with the breakup of Gondwana in the Early Jurassic.

Dwyka Group

The basal unit in the Karoo Supergroup accumulated under glacial conditions and is comprised primarily of diamictite and shale. The Dwyka is divided into two lithofacies, the Northern valley/inlet facies and the Southern platform facies (Smith et al., 1993). The valley/inlet facies was deposited in paleovalleys, now located around the northern margin of the basin, and consists of interbedded mudstone, diamictite, conglomerate, and pebbly sandstone. This interval is a seemingly random assortment of sub- and supraglacial remnants that aggraded in the topographic lows of the glaciated craton during the Late Carboniferous to Early Permian (Johnson et al., 2006). The platform facies found in the southwestern basin contains a sequence of massive diamictite from grounded or floating ice sheets that were deposited in subaqueous environments. Several glacial/interglacial cycles are recorded in this unit. As Gondwana drifted away from the pole, offshore, fully marine mud was deposited over the diamictite; these shales cap the Dwyka Group.

Ecca Group

Overlying the glaciogenic Dwyka Group in an "abrupt but diachronous contact" is the Ecca Group (Smith et al., 1993). Deposits in this unit resulted from suspension settling of sediments, turbidite flows, and progradation of deltas. Following deglaciation, a "shallow" epicontinental sea occupied the basin and low-energy fluvial systems began building deltas into this water body. The sea had a broad, shallow shelf dominated by silt and mud sediments. The Karoo Trough to the south and Natal Trough to the east both filled with flysch deposits. In the southern Karoo, the Ecca reaches thicknesses of 1000 m and consists of seven formations. The

Prince Albert and Whitehill formations are primarily mudstone and shale. The black shale of the Whitehill Formation indicates that it was deposited in an anoxic environment, such as in the bottom waters of the epicontinental sea (Smith et al., 1993). Overlying these deposits is the Collingham Formation, representing distal turbidites. The Vischkuil and Laingsburg formations record an overall coarsening up sequence into proximal turbidite deposits as the basin continued to fill. The Fort Brown Formation records the introduction of prodelta mud into the Karoo Sea and coastal progradation continued into the Waterford Formation. The Waterford is comprised of delta-front and delta-plain sand and mud (Pludow et al., 2010; Kapupu et al., 2010), and is interpreted as the final infilling phase of the epicontinental sea.

Beaufort Group

The Beaufort Group represents the transition to fully subaerial deposition and predominantly fluvial sedimentation beginning in the Middle Permian. The sequence continues into the Early Triassic and spans the Permian-Triassic Boundary (PTB), reaching thicknesses in excess of 3 km. It is marked by alternating mudstone and sandstone with an overall fining-upwards character. These sediments accumulated in response to floodplain aggradation on semi-arid braidplains (Smith et al., 1993). The Beaufort Group consists of two Subgroups, the Lower Adelaide and Upper Tarkastad, which have been subdivided into six and three formations, respectively.

The lowermost units of the Adelaide are the Abrahamskraal Formation in the west and the Koonap Formation in the southeast interpreted to represent upper delta plain overbank and mudflat deposits, formed in response to the flooding of meandering rivers flowing to the remnants of the Ecca Sea sourced from the Cape Fold Belt (Johnson et al., 2006). These are overlain by the Teekloof and Middleton formations, respectively. The contact represents a

floodplain facies association through which ephemeral rivers deposited sediment. The climate under which these sediments were deposited is interpreted as semi-arid colonized by riparian vegetation (Smith et al., 1993). The Balfour Formation is the uppermost unit of the Adelaide Subgroup in the southeast and spans the PTB. In the northeast, beyond the extent of this study, is the coeval Estcourt Formation.

The Tarkastad Subgroup begins with the Katberg Sandstone Member in the east, which occurs directly above the Teekloof Formation. The Katberg can reach thicknesses of 1000 m and is arenaceous with less than 10% of the clastic sediments finer than sand-sized grains. It represents barforms and paleosols in a braidplain setting (Pace et al., 2009). The Katberg is considered equivalent to the Belmont Formation found elsewhere in the basin. Above the Katberg is the Burgersdorp Formation which consists of mudrocks with ephemeral stream sandstones.

Molteno Formation

Middle Triassic deposits are assigned to the Molteno Formation. This is a predominantly sandstone unit that fines upwards from coarse to fine clasts and represents deposition in a bedload dominated fluvial wedge (Smith et al., 1993). These sediments were deposited in response to uplift caused by rifting tied to the early breakup of Gondwana. The climate under which the Molteno was deposited was cool-temperate and wet.

Elliot Formation

The distinctive “red bed” mudrock and sandstone of the Elliot Formation are Late Triassic deposits of ephemeral streams and floodplain playas (Smith et al., 2003). Climate became increasingly arid and these rocks are interpreted to represent the distal equivalent of the Molteno braided deposits.

Clarens Formation

The Clarens Formation is generally composed of fine, calcareous sandstone and was deposited in the Late Triassic to Early Jurassic primarily in sand dunes (Smith et al., 2003). This unit is a combination of aqueous and eolian sediments, and distal alluvial fan complexes.

Drakensberg Volcanics

Debate exists rearding the timing of the transition between the Clarens sediments and the overlying Drakensberg volcanics. These volcanic flows lie atop different stratigraphic units in various parts of the basin leading authors to speculate that the relationship may be diachronous (Smith et al., 1993). These Late Triassic to Early Cretaceous flood basalts and pyroclastics are linked to the breakup of Gondwana, and arose through partial mantle melt followed by convective upwelling. An initial explosive phase of pyroclastic breccias and tuffs is followed by effusive basaltic flows. These deposits have led to hypotheses that the breakup of Gondwana began in the east in the Late Triassic and reached the west in the Early Cretaceous.

Pedogenic Mud Aggregates

Terrestrial paleoclimate proxies are developed from the sedimentary character of alluvial deposits in the stratigraphic record. One of the most widely used proxies for non-marine sediments is paleosols, which are ancient soils that have been lithified and included in the rock record. Their lithological and chemical features can provide insight into characteristics of the soil during the period of deposition and soil formation which can, in turn, detail paleoclimate because soils form under very specific conditions. In seasonally controlled soils, the development of a pedogenic feature known as an aggregate may form. These structures develop when swelling clays are alternately wetted and dried resulting in the formation of sand-sized aggregates (62.5 μm - 2 mm) of mud-sized clasts (<3.9 μm). These features can be recognized in thin sections of

in situ soil profiles and as reworked clasts in river deposits. Aggregates have been identified in both ancient and modern soils and coeval river deposits (Müller et al., 2004).

Modern Occurrences

Pedogenic mud aggregates have been identified in active fluvial systems in the Lake Eyre Basin of Australia (Figure 3), particularly in Cooper Creek and the Diamantina River (Rust and Nanson, 1989). These are two of the three major rivers that drain the basin and they are characterized by low slopes and primarily braided channels. The fact that their sediment load is primarily mud is an apparent anomaly with the braided character of their channels. This discrepancy is explained by the abundance of aggregates in soils and bedload. Formation of these aggregates is linked to the complex of cracks that form on the floodplains during dry periods. These cracks are up to 1 m deep and are separated from one another by distances up to tens of meters.

Modern floodplain soils of the Lake Eyre Basin are roughly comparable to Vertisols in the rock record and are characterized as deeply cracked grey soils. Their swelling clay component is primarily kaolinite which differs from the smectite-dominated Vertisols (Rust and Nanson, 1989). The presence of these expandable clays is what allows for the formation of the crack network on the surface during shrinking and swelling in drought/flood cycles, respectively.

Rust and Nanson (1989) assert that the crack network is necessary to the entrainment of aggregates in bedload. During rainfall, water falls into the cracks and soil masses fall into the water. The soil then is separated into aggregates which are transported through the cracks. Once formed, the aggregates are then available for transport during the next flood event where they are easily entrained because of their lower density than mineral grains. Aggregates likely accumulate on floodplains along with quartz grains and pore space is then infiltrated by suspended clay

during flood events. Based on the Australian study, an environment must be dry enough to produce a crack network in order to generate pedogenic mud aggregates.

Ancient Occurrences

Aggregates are considered a good climate proxy because the rainfall, temperature, and clay mineralogical conditions required for their formation are well constrained. They are also valuable because they have been demonstrated to retain their texture even when reworked or buried up to 3000 m depth; hence, preservation potential is high (Müller et al., 2004). Rust and Nanson (1989) and Wright and Marriott (2007) demonstrated that mud-sized particles occur as bedload when included in silt-sized aggregates. The presence of aggregates in fluvial deposits indicates that climatically stable periods of aggradation on the floodplain were interspersed with periods of degradation, reworking, and redeposition. This can be separated from the natural migration of a river channel by differences in sediment type when a comparison is made between overbank and channel deposits.

Aggregates have been reported from a variety of study areas spread geographically and through geologic time. Rust and Nanson (1989) reported modern aggregates forming on floodplains of the Lake Eyre Basin of Australia. Gierlowski-Kordesch and Gibling (2002) found aggregates in the New-Haven Arkose of the Hartford rift basin, Connecticut, of Triassic-Jurassic age. Aggregates were documented in the Upper Triassic Lunde Formation in the North Sea by Müller et al. (2004). Wright and Marriott (2007) have reported aggregates in the Lower Old Red Sandstone in Wales which dates from the late Silurian to early Devonian.

All documented instances of pedogenic mud aggregates in the rock record are reported exclusively from Vertisol soil profiles. A Vertisol is defined, under the classification of Mack et al. (1993), as a paleosol characterized by extensive pedoturbation made possible by a high

concentration of swelling clays, especially smectite. This pedoturbation may result in features such as dessication cracks, wedge-shaped peds, hummock-and-swale structures, slickensides, and clastic dikes (Mack et al., 1993). It is generally difficult to identify a Vertisol based only on clay mineralogy because the minerals are often converted during diagenesis so a combination of these characteristics is often necessary.

Application to the Karoo Basin

The mudclast aggregate proxy has yet to be applied to the Karoo Basin where it could serve an important function in comparing climates across the PTB. The Middle Permian was marked by deglaciation of Gondwana and a changeover from submarine to fully terrestrial deposition. The presence of mud aggregates in basal lag deposits from the Abrahamskraal Formation would indicate a seasonal climate with bedload dominated fluvial systems. Similarly, the presence of these features in the Lower Triassic would substantiate claims of an arid climate following the boundary event.

Uncertainties about the prevailing environmental conditions in older Karoo sequence rocks also exist. Scheffler et al. (2006) use a geochemical model to suggest a warm-arid to warm-humid environment during deposition of the Abrahamskraal Formation with a shift to oxic conditions across the PTB. Others studies have found evidence of landscapes dominated by wetland soils in the Lower Triassic (Gastaldo and Rolerson, 2008), while other soils indicate deposition under more seasonal conditions with evidence for these restricted to braided river deposits (Pace et al., 2009). Other hypotheses for the Early Triassic are alternately of increasing aridity, based on the fluvial record, (Ward et al., 2005) or humidity, based on the absence of fossil plants (Retallack et al., 2003). However, it is important to note that there are discrepancies in the palesosol types identified by Retallack et al. (2003) in the Early Triassic and those

identified by this author in the field, which suggests that their climate hypothesis may be questionable.

To date, aggregates from the rock record at other localities have been identified exclusively in Vertisols, which demonstrate pedohomogenization in response to expansion and contraction of swelling clays. The presence of Vertisols and associated mud aggregates are interpreted as representative of a wetted/dried landscape (Mack et al., 1993). However, as no Vertisols have been recorded from the Lower Triassic, to date, the presence of aggregates of this age in the Karoo Basin stratigraphy would indicate either that Vertisols were once present and have since been eroded or that aggregates can form in other soil types and other environments.

The identification of pedogenic mud aggregates in the Middle Permian and Lower Triassic of the Karoo Basin has several implications. First, their presence will provide more information about prevailing climates during each of these intervals, testing ideas of other workers (e.g., Ward et al., 2005; Retallack et al., 2003; Pace et al., 2009). Second, identifying differences and similarities between different age deposits will help to clarify environmental changes before and after the PTB. Finally, if mud aggregates occur in both sequences, determining the clay mineralogy will either provide evidence for the possibility of Vertisols having been present on these landscapes or suggest that aggregates can form in other soil types.

MATERIALS AND METHODS

Samples from the Katberg Formation were collected from Carlton Heights in the Eastern Cape Province (31° 17.702’ S, 24° 57.093’ E) by both Dan Pace ’07 and the author. This formation represents deposits of a braided, low sinuosity river system (Pace et al., 2009) within paleosols identified as originating in a wetland environment (Gastaldo and Rolerson, 2008). The

area sampled is exposed along a roadcut of the N-9 highway. Nine samples were collected from intrachannel mudchip conglomerate deposits and four from paleosols (Figures 4 & 5). Siltstone samples 1a and 1b were collected from directly beneath the second sandstone (SS2) of Pace et al. (2009). Sample 2 was collected from the *Katbergia* soil horizon of Gastaldo and Rolerson (2008). Samples 3 and 4 were collected from the siltstone between SS2 and SS3. Samples 5-13 were collected from mudchip conglomerates within barforms in the channel deposits of SS3 (Pace et al., 2009). Three siltstone samples were taken from each of three mudchip conglomerate lenses. The conglomeratic lag samples studied were collected by Pace and originated from the conglomerate basal to their SS3.

Middle Permian samples of a lithologic character similar to the Triassic conglomeratic lag were collected from the Abrahamskraal Formation near Sutherland, Northern Cape Province (32° 31.802’ S, 20° 37.854’E). The Abrahamskraal Formation is the basal unit of the Beaufort Group and the interval is interpreted to represent fully terrestrial deposition in high sinuosity rivers under a seasonal to arid climate (Johnson et al., 2006). Samples are from a conglomeratic lag at the base of a multistory and multilateral sandstone exposed along the R354 in Verlatenkloof Pass (Katsiaficas et al., 2010; Figures 6 and 7).

Thin sections of all samples were prepared by the author as well as Applied Petrographic Services (APS) (Figure 8). Those slides made by APS were filled with blue epoxy to facilitate identification of pore space (Figure 9). Where hand-sample sized blocks could be collected, stratigraphic “up” was marked with an arrow and notch on the slide. However, for many of the samples, particularly those from paleosol deposits, poor cementation and extensive weathering resulted in samples consisting of siltstone fragments and slivers where stratigraphic direction

could not be determined. Additionally, thin section slides created by Pace do not have stratigraphic up indicated.

Examination at both the macroscopic and microscopic scale was conducted in the search for aggregates of clay-sized particles. Macroscale identification at low magnification was primarily accomplished with a hand lens as well as a Leitz macroscope. Microscale studies were completed under plane- and cross-polarized light on a Nikon petrographic microscope at 40x and 100x magnification. Once aggregates, as well as control-group quartz grains, were identified, their diameters were measured using NIS-Elements image processing software (Figure 10). The inclusion of a control group was important to compare the size of identified aggregates to other grains in the samples. Quartz grains were selected for the control group because of ease of identification, well constrained mineralogy information (e.g., density), and their abundance in the samples. Sample size was 300 grains each for channel aggregates, quartz, and paleosol quartz, and was 100 for paleosol aggregates. Aggregates could be differentiated from quartz grains based primarily on their brown to gray appearance in both plane and cross-polarized light. Quartz grains are clear in plane polarized light and show first-order gray birefringence. Quartz grains tend to be more angular than aggregates and both are surrounded by silt matrix or pore space.

In addition to petrographic analysis, SEM analysis was undertaken to determine clay mineralogy to ascertain composition of the aggregates clasts and mineral grains surrounding them. This data collection, completed at the University of Maine at Orono, used an AMRay 1820 with standardless samples run at 20 kV. Samples were not carbon coated. Back-scatter electron images were collected for samples from Carlton Heights channel, paleosol, and conglomerate deposits, and from Sutherland conglomerate deposits (Figures 11, 12, 13, and 14). Semi-

quantitative chemical data also were collected from the SEM, from which information about aggregate mineralogy was gathered.

RESULTS

Identified aggregates conform to criteria based upon the studies of other authors, (e.g., Müller et al., 2004; Gierlowski-Kordesch and Gibling, 2002; Ékes, 1993; Rust and Nanson, 1989) designed to facilitate their identification in thin section. These criteria include: each aggregate having an individual, unique shape, and not simply filling pore space between other grains as matrix material; and each aggregate containing several clay clasts within its boundaries, indicating that this grain is truly an aggregate. Size criteria were based on the size of surrounding clasts and these grains were expected to be similar in size, while shape of aggregates was expected to be subangular to subrounded (Figure 9). Chemical composition was also an important criterion, and clay mineralogy was expected to reflect a swelling clay rich composition.

Carlton Heights Lithologies

The Lower Triassic Katberg Formation exposure at Carlton Heights was characterized by Pace et al. (2009) and interpreted as a multilateral and multistory fluvial deposit. Four lithofacies are identified and can be grouped into channel and interchannel deposits. Lowest in the stratigraphy are siltstone intervals that are interpreted as overbank fines that have undergone pedogenesis which is evidenced by bioturbation of *Katbergia* (Gastaldo and Rolerson, 2008). It is from this unit that paleosol samples (samples CH09-01 – CH09-04) were collected for this study. These are overlain by a very fine-grained feldspathic wacke interpreted as sheetflood deposits. These two lithofacies are interbedded until the introduction of the pedogenic nodule

conglomerate facies, signifying the beginning of channel deposition. These conglomerates, with pisolith-size nodules, are found above erosional channel bases and range in thickness from 0.03 to 1 m. It is from these conglomerates that the conglomeratic lag samples from this study originate (sample PC1). Above the lag deposits are channel barform deposits which consist of a fine-grained wacke and a pebble-mudstone conglomerate. Channel samples for this study were collected from the pebble-mudstone conglomerate (samples CH09-05 – CH09-13). Channel deposits consisting of the conglomerate and fine-grained wacke lithofacies are interbedded with the bioturbated siltstone and very fine-grained wacke throughout the section.

Sediment Load

The diameter of aggregates identified in the pebble-mudstone conglomerate facies of channel deposits ranges from 44 μm to 270 μm with an average of 126 μm. Channel-quartz clasts range from 16 μm to 327 μm with an average size of 98 μm (Appendix 1). Both of these averages fit within the fine sand-size classification. Distribution of grain size indicates that quartz is predominantly of fine sand while aggregates are skewed towards fine and medium sand-sized clasts (Figure 10).

Aggregates were also identified in paleosol deposits (the siltstone intervals of Pace et al., 2009). Size and shape of aggregates in Carlton Heights channel and paleosol deposits are indistinguishable in thin section. Although there is variance in size and shape, the overlap in this range makes it to impossible to separate individual aggregates by origin based on petrographic analysis alone. Fewer aggregates were found in paleosol deposits, and the sample size was restricted to 100 measurements. Paleosol-aggregate diameter ranged from 47 μm to 228 μm, with an average of 107 μm. Size of the 300 measured quartz grains ranged from 16 μm to 235 μm, with an average size of 67 μm (Appendix 1). Paleosol-quartz grains were distributed more evenly

across grain size categories than their channel counterparts. Paleosol aggregates had a mode size of fine grained clasts, which is a smaller predominate grain size than channel aggregates (Figure 10).

Sedimentary Structures

Attempts were made to apply the criteria of Wright and Marriott (2007) to the samples of this study, but the limited extent of mudrock units and absence of structures within these units made this method of identification unsuccessful.

Microscale Structures

Successful identification of pedogenic mud aggregates took place at the microscale through petrographic analysis. This was accomplished by identifying grains with a size similar to surrounding quartz and feldspar grains but that were gray-brown in both plane- and cross-polarized light. Shape of aggregates was well defined and generally sub-rounded. Aggregates were composed of many smaller grains (Figure 9). Identification was facilitated if an aggregate was surrounded by pore space. During thin section preparation, pore space was filled with blue epoxy, making aggregates that were surrounded by voids obvious. Preservation potential was increased where aggregates were surrounded by quartz grains which had preserved their shape and kept them from being crushed during compaction. These criteria were met by many clasts (>300) in the channel deposits. Aggregates also were identified in paleosols and conglomeratic lags from the Early Triassic, although they were not as abundant. Figures 11, 12, 13, and 14 illustrate typical aggregates from each of these depositional settings.

Aggregate Mineralogy

Semi-quantitative oxide data were gathered for aggregates identified in thin sections of paleosol (sample CH09-01B), channel (sample CH09-05), and conglomerate lag (sample PC1

from Carlton Heights and 010610.2 from Sutherland) deposits (Figure 8; Appendix 2). The clay mineralogy of aggregates could not be differentiated at high resolution because of limitations on data collection, but aggregates tended to have a fairly homogeneous composition. Specific clay grains within aggregates, as well as averages for the entire clast, resulted in virtually identical data. Paleosol-and-channel spectra distributions were very similar to one another with significant EDS spectral peaks of SiO_2 (~60 wt%) and Al_2O_3 (>20 wt%, Figure 15). Other peaks included K_2O, FeO, MgO, and Na_2O at <10 wt% each (Figure 15). The two Carlton Heights conglomerate samples had a similar composition to the paleosol and channel samples with the addition of a carbon peak (Figure 15). In addition, the second aggregate sampled (Figure 15) shows a much higher CaO component (22 wt%) than any of the other Carlton Heights samples.

For each aggregate, neighboring minerals also were analyzed, although these EDS spectra are not shown. The mineralogy of surrounding clasts was exclusively quartz, potassium feldspar, and a range of plagioclase feldspar compositions.

Abrahamskraal Formation

Katsiaficas et al. (2010) have outlined and interpreted the lithologies and sedimentary structures found at the Abrahamskraal Formation roadcut near Sutherland. This outcrop consists of five lithofacies: a bedded siltstone, a bioturbated siltstone, a coarse siltstone, a lithofeldspathic wacke, and a silt-pebble conglomerate. These facies represent deposition under terrestrial conditions and Katsiaficas et al. (2010) interpret the sequence as a basal floodplain paleosol that has been scoured into by the migration of a meandering, high-sinuosity fluvial system. Channel fill deposits include a basal scour overlain by fine-grained sandstone barforms organized into at least 5 channels. This is topped by a sequence that fines up to a siltstone that has undergone pedogenesis.

Specimens from the Abrahamskraal Formation outcrop did not exhibit any macroscopic indicators of pedogenic mud aggregates. Samples of the roadcut conglomerate were then inspected in thin section and potential aggregates were identified (Figure 14). Clasts that fit the microscale criteria outlined by (Müller et al., 2004) were less common than in any of the Carlton Heights samples. Although some grains appeared brown in both plane and cross-polarized light and seemed to be composed of several clasts aggregated together, chemical studies determined that the majority of the sample consisted of quartz and feldspar grains as well as lithic fragments. Examination with the SEM demonstrated that these grains were, rather than mudclasts, discolored aggregates of quartz and feldspars (Figure 14). Subhedral pyrite crystals were identified under reflected light studies of thin section slides. Based on these samples, there is no indication of pedogenic mud aggregates in the Abrahamskraal Formation samples from near Sutherland.

DISCUSSION

A comparison of pedogenic-derived carbonate nodule-bearing conglomerate from the Middle Permian Abrahamskraal Formation and the Lower Triassic Katberg Formation indicate that no aggregates are present in Middle Permian paleosols but that they formed in Early Triassic soils, indicating a difference in environmental conditions. It was not possible to identify mudclast aggregates using macroscopic features as described by other workers (Wright and Marriott, 2007) at any of the localities because of a lack of macroscale structures in the outcrops. It was only when thin sections of lithofacies were examined that microscopic criteria used by Müller et al. (2004) allowed for identification of aggregates. Of the criteria employed by others, those that could be applied to this study include an aggregate size similar to other grains,

subrounded shape, and composition including several mud clasts. Constraints of the outcrop and sediment nature at the Lower Triassic Carlton Heights locality restrict the criteria that can be employed. None of the criteria could be applied to the R354 outcrop of Middle Permian age. Rather, although each channel lag deposit appears similar in gross features, upon closer inspection, the pedogenic mud aggregates could be identified in the Lower Triassic but not Middle Permian samples.

Carlton Heights Aggregates

The EDS spectra of confirmed aggregates from Carlton Heights lithofacies give insight into the processes taking place in this environment in the Early Triassic. Both similarities and differences in chemical composition of mud aggregates are important to consider, even if exact mineralogy cannot be determined. Bulk chemistry of paleosol and channel aggregates were nearly identical with similar peaks of Si, Al, K, Mg, Na, and Fe (Figure 15, 16; Appendix 2). The presence of chemically similar aggregates indicates that aggregates residing in the channel deposits were deposited there through erosion and reworking of the adjacent paleosol deposits based on bulk chemistry and similarity of appearance.

These similarities also indicate that aggregates formed in paleosols, in which there is no physical evidence for development of Vertisol features. Pace et al. (2009) identify Gleysols, Inceptisols, and Calcisols and evidence for eroded Aridisols in the Carlton Heights outcrop, but there is no evidence for any Vertisol present in their stratigraphy. All other pedogenic mud aggregates have been identified from Vertisol profiles. The chemical similarities between aggregates of the paleosol and channel reaffirm the hypothesis that erosion of the existing paleosols was responsible for deposition of aggregates in the channel and also confirm that these aggregates can form in a variety of soil types.

The differences between the chemical makeup of paleosol-and-channel aggregates and conglomerate lag aggregates are just as significant as the similarities discussed above. This second, unique, chemistry found in the conglomerates suggests that a second generation of aggregates was also deposited in the fluvial system at Carlton Heights. The different dominant peaks in both conglomerate aggregates sampled (greater calcium and carbon peaks) indicate a different clay chemistry in conglomerate aggregates than in channel and paleosol aggregates. Since the conglomerate is stratigraphically lower than the sandstone channel bars, the aggregates with a stronger carbon signature found in this unit (Figure 13; Appendix 2) must have been eroded from an older paleosol deposit which existed on the landscape before the paleosol which is still present at the outcrop. The now absent paleosol, which may have been a Vertisol (although this cannot be determined due to a lack of conclusive mineralogy) was likely removed from the landscape during the degradational portion of the cycle described by Pace et al. (2009). However, by examining the conglomeratic lag deposits, remanants of this paleosol can be found. This evidence of a chemical signature different from those still preserved in the outcrop is further evidence for the removal of soil profiles from the early Triassic deposits at Carlton Heights.

These two disparate chemical signatures from Carlton Heights indicate two generations of aggregates that formed at this site. A younger paleosol deposit resulted in more carbon rich aggregates which are deposited in the basal-most conglomeratic lag deposits. Once this paleosol had been eroded, the channel began to erode into lower paleosols which are still preserved in outcrop. The aggregates in paleosol-and-channel deposits have a nearly identical chemistry, indicating erosion from the neighboring paleosol sourced the aggregates for the channel deposition.

Abrahamskraal Formation

Despite the initial microscale identification of pedogenic mud aggregates in a Middle Permian Abrahamskraal Formation lag conglomerate, upon closer investigation it was determined that there were no mud aggregates in these samples. The clasts thought to mimic aggregates had similar color and shape characteristics under polarizing light microscopy, but upon chemical analysis were shown not to be of clay composition. This information indicates differences between the two study areas. Although the presence of mud aggregates is not diagnostic of specific environmental conditions, their absence in these Middle Permian deposits means there are differences between the paleosols that developed in the Sutherland and Carlton Heights localities.

Examination of conglomerate samples from the R354 outcrop verified the findings of Katsiaficas et al. (2010). This conglomerate represents basal-most deposition in a meandering fluvial system. The presence of pyrite in Sutherland samples is unrelated to the development of pedogenic mud aggregates, and its identification suggests anoxic diagenetic conditions. It is also an important discovery in terms of constraining chemical data. By considering the known chemical formula of pyrite (FeS_2), an expected EDS spectrum would include only Fe and S peaks. By comparing this expectation to the actual EDS spectrum analysis produced for the grain (Figure 16), a qualitative determination of error in aggregate EDS spectra can be determined by observing the magnitude of the other, unexpected, peaks. These samples were not carbon coated prior to analysis and there was a greater "skirting effect" of surrounding grains. Hence, rather than only the area of interest being sampled, neighboring grains had an impact on the resultant chemical spectra produced. This is significant because it indicates the level of error that is present in the EDS spectra of aggregates. Although this error cannot be quantified in the present

study, it is important to consider that neighboring grains play a role in the chemical analysis of these samples.

Middle Permian to Early Triassic Transition

Based on differences in the sedimentological character of the Permian and Early Triassic, there has long been proposed a changeover in fluvial styles across the PTB. Researchers interpret that the fluvial systems that dominated the Karoo Basin from the Late Permian onwards shifted from high-sinuosity channels to bedload dominated, low-sinuosity channels (Stear, 1978; Stear, 1983; Hiller and Stavrakis, 1984; Smith, 1995). Ward et al. (2000) support this hypothesis with the identification of three principal lithofacies, one occurring before, one coinciding with, and one occurring after the PTB. Below the boundary is a sandstone interval formed by channel scouring. Sedimentation occurs in a unidirectional flow, and is interpreted as deposition in meandering fluvial systems. A basin-wide laminated sandstone-shale unit is hypothesized to occur at the boundary by Ward et al. (2000), although this has since been disproved by Gastaldo et al. (2009). A braided facies is identified above the PTB by an interval with a higher sandstone proportion and the presence of multistoried and vertically accreted channels, indicating higher sedimentation rates in a braided system.

This change in fluvial systems has been interpreted to reflect a change in environmental conditions across the PTB. There are a variety of ideas regarding what mechanism controlled the changeover including tectonic thrusting (Smith, 1995) and rejuvenation (Hiller and Stavrakis, 1984), or a rapid die-off of vegetation across the landscape, resulting in increased erosion rates (Ward et al., 2000). But Gastaldo et al. (2005) point out that the changeover in plant fossils preserved can be attributed to a change in taphonomic regime across the PTB rather than actual biodiversity loss. Despite differing hypotheses about the responsible mechanism, these authors

agree that there was a general drying and warming trend beginning in the Late Permian and lasting into the Early Triassic accompanied by a shift to more oxic conditions (Scheffler, 2006).

The proposed differences between Middle Permian and Early Triassic environments in the Karoo Basin are further understood by the data collected in this study. Previous hypotheses of a wetter and cooler climate in the Permian (Ward et al., 2005) are supported by the absence of mud aggregates in samples from the Abrahamskraal Formation. The proposed climate of the Late Permian is that of an environment lacking the wetting and drying cycles that are essential to the formation of pedogenic mud aggregates as presently understood (Rust and Nanson, 1989). Increasing aridity in the Triassic, in conjunction with the introduction of swelling clays in the soil profile, would be required to produce the aggregates identified in early Triassic samples.

Significance for Fluvial Style

The presence of aggregates in river deposits has important ramifications for understanding the type of rivers that crossed the land surface and, thus, climatological and environmental parameters. The presence of pedogenic mud aggregates in channel deposits means that silt-sized clasts were transported as bedload, not just as suspended load, which provides information about the qualities of the river system.

The modern analog for fluvial systems in which pedogenic mud aggregates now are being deposited is the Channel Country of Australia. This area in the Lake Eyre Basin is comprised of braided and anastamosing fluvial channels with a sediment load of primarily mud in a semi-arid environment. Nanson et al. (1986) first identified the formation of aggregates in floodplains, and their transport and retention in fluvial systems that cross the basin.

The characteristics of dryland rivers in which pedogenic aggregates occur are outlined by Nanson et al. (1986). These systems are characterized by seasonal rainfall that runs off quickly

and the presence of floods at a variety of scales including flash, single-peak, multiple-peak, and sustained seasonal floods. Flow can vary widely in these systems, and is more dependent upon short-term variability in rainfall than larger-scale averages. What has long been considered a specific and unique fluvial environment actually represents a continuum of fluvial types. Cooper River, in western Queensland's Channel Country, has much of its bedload comprised of pedogenic mud aggregates which form ripples and dunes (Maroulis and Nanson, 1996). Maroulis and Nanson (1996) emphasize that the volume of information that is known about dryland rivers in general is far inferior to the volume of the questions that remain. There is extreme variability in the characteristics of sediment transport, the role of vegetation, and sensitivity to climate change. Additionally, hypotheses for dryland rivers are based on a very small subset of the dryland rivers in existence. Nonetheless, these bedload dominated, anabranching systems with a significant proportion of mud aggregates transported as bedload are the best modern analog for the early Triassic Carlton Heights outcrop based on sedimentologic similarities. By better understanding the variation in modern environments in which pedogenic mud aggregates can form it may be possible to better constrain the landscape upon which these aggregates formed in the Early Triassic.

CONCLUSIONS

The research of other authors in both modern and ancient settings has demonstrated the formation of pedogenic mud aggregates in semi-arid conditions. Their presence in channel deposits indicates the transport of sand-sized clasts in bedload although the material is actually composed of mud-sized grains. Based on the identification criteria of other authors including size, shape, and composition of grains, samples from the Early Triassic were compared to

Middle Permian samples based on petrographic characteristics and using chemical composition to determine the presence of aggregates in these strata.

Chemical analysis of Carlton Heights channel deposits identifies two generations of aggregates. One of these generations matches those aggregates in paleosol deposits adjacent to the channel deposits. The other aggregate signature does not match any sampled aggregate, indicating it originated in a now-eroded paleosol. The presence of mud aggregates in the Early Triassic fluvial deposits means that bedload capacity was higher than would be expected from only considering sand-sized clasts, which provides insight into fluvial changeover after the PTB at 252.6 Ma. A demonstrated change in fluvial type from high- to low-sinuosity systems coincides with an increase in aridity as evidenced by the formation of pedogenic mud aggregates in younger deposits.

REFERENCES

DeKock, M.O., and Kirschvink, J.L., 2004, Paleomagnetic Constraints on the Permian-Triassic Boundary in Terrestrial Strata of the Karoo Supergroup, South Africa: Implications for Causes of the End-Permian Extinction Event: Gondwana Research, v. 7, p. 175-183.

Ékes, C., 1993, Bedload-transported pedogenic mud aggregates in the Lower Old Red Sandstone in southwest Wales: Journal of the Geological Society, London, v. 150, p. 469-471.

Gastaldo, R.A., and Rolerson, M.W., 2008, *Katbergia* gen. nov., a new trace fossil from the Late Permian and Early Triassic of the Karoo Basin: Implications for paleoenvironmental conditions at the P/Tr extinction event: Palaeontology, v. 51, p. 215-229.

Gastaldo, R.A., Neveling, J., Clark, K.C., and Newbury, S.S., 2009, The terrestrial Permian-Triassic boundary event bed is a non-event: Geology, v. 37, p. 199-202.

Gastaldo, R.A., Adendorf, R., Bamford, M., Labandeira, C.C., Neveling, J., and Sims H., 2005, Taphonomic trends of macrofloral assemblages across the Permian-Triassic Boundary, Karoo Basin, South Africa: PALAIOS, v. 20, p. 479-497.

Gierlowski-Kordesch, E.H., and Gibling, M.R., 2002, Pedogenic mud aggregates in rift sedimentation: *in* Renaut, R.W., and Ashley, G.M., eds., Sedimentation in Continental Rifts: SEPM Special Publication, v. 73, p. 195-206

Hiller, N., and Stavrakis, N., 1984, Permo-Triassic fluvial systems in the southeastern Karoo Basin, South Africa: Palaeogeography, Palaeoclimatology, Palaeoecology, v. 45, p. 1-21.

Johnson, M.R., van Vuuren, C.J., Visser, J.N.J., Cole, D.I., Wickens, H. de V., Christie, A.D.M., Roberts, D.L., and Brandl, G., 2006, Sedimentary rocks of the Karoo Supergroup: *in* Johnson, M.R., Anhaeusserm, C.R., and Thomas, R.J., eds., The Geology of South

Africa: Geological Society of South Africa, Johannesburg, Council for Geoscience, Pretoria, p.461-495.

Kapupu, C., Gastaldo, R.A., and Neveling, J., 2010, The lithological characterization of a Middle Permian deltaic distributary channel, in the Karoo Basin, South Africa: Geological Society of America Abstracts with Programs, v. 42, p. 428.

Katsiaficas, N., Gastaldo, R.A., and Neveling, J., 2010, An analysis of geometric and sedimentologic characteristics of a Middle Permian fluvial system, Karoo Basin, South Africa: Geological Society of America Abstracts with Programs, v. 42, p. 428.

Mack, G.H., James, W.C., and Monger, H.C., 1993, Classification of paleosols: Geological Society of America Bulletin, v. 105, p. 129-136.

MacLeod, K.G., Smith, R.M.H., Koch, P.L., and Ward, P.D., 2000, Timing in mammal-like reptile extinctions across the Permian-Triassic boundary in South Africa: Geology, v. 28, p. 227-230.

Maroulis, J.C., and Nanson, G.C., 1996, Bedload transport of aggregated muddy alluvium from Cooper Creek, central Australia: a flume study: Sedimentology, v. 43, p. 771-790.

Müller, R., Nystuen, J.P., and Wright, V.P., 2004, Pedogenic mud aggregates and paleosol development in ancient dryland river systems: criteria for interpreting alluvial mudrock origin and floodplain dynamics: Journal of Sedimentary Research, v. 74, p. 537-551.

Mundil, R., Ludwig, K.R., Metcalfe, I., and Renne, P.R., 2004, Age and timing of the Permian mass extinctions: U/Pb dating of closed system zircons: Science, v. 305, p. 1760-1763.

Nanson, G.C., Tooth, S., and Knighton, A.D., 2002, A global perspective on dryland rivers: Perceptions, misconceptions and distinctions: *in* Bull, L.J., and Kirkby, M.J., eds.,

Dryland Rivers: Hydrology and Geomorphology of Semi-arid Channels: John Wiley and Sons, p. 17-54.

Pace, D.W., Gastaldo, R.A., and Neveling, J., 2009, Early Triassic aggradational and degradational landscapes of the Karoo basin and evidence for climate oscillation following the P-Tr Event: Journal of Sedimentary Research, v. 79, p. 316-331.

Pludow, B.A., Gastaldo, R.A., and Neveling, J., 2010, A Middle Permian (Wordian) avulsion system, Karoo Basin, South Africa: Implications of the Ecca-Beaufort transition: Geological Society of America Abstracts with Program, v. 42, p. 428.

Retallack, G.J., Smith, R.M.H., and Ward, P.D., 2003, Vertebrate extinction across Permian-Triassic boundary in Karoo Basin, South Africa: Geological Society of America Bulletin, v. 115, p. 1133-1152.

Rust, B.R., and Nanson, G.C., 1989, Bedload transport of mud as pedogenic mud aggregates in modern and ancient rivers: Sedimentology, v. 36, p. 291-306.

Scheffler, K., Buehmann, D., Schwark, L., 2006, Analysis of late Palaeozoic glacial to postglacial sedimentary successions in South Africa by geochemical proxies- Response to climate evolution and sedimentary environment: Palaeogeography, Palaeoclimatology, Palaeoecology, v. 240, p. 184-203.

Smith, R.M.H., 1995, Changing fluvial environments across the Permian-Triassic boundary in the Karoo Basin, South Africa, and possible causes of tetrapod extinctions: Palaeogeography, Palaeoclimatology, Palaeoecology, v. 117, p. 81-104.

Smith, R.M.H., Eriksson, P.G., and Botha, W.J., 1993, A review of the stratigraphy and sedimentary environments of the Karoo-aged basins of Southern Africa: Journal of African Earth Sciences, v. 16, p. 143-169.

Stear, W.M., 1983, Morphological characteristics of ephemeral stream channels and overbank splay sandstone bodies in the Permian Lower Beaufort Group, Karoo Basin, South Africa: International Association of Sedimentologists Special Publications, v. 4, p. 405-420.

Stear, W.M., 1978, Sedimentary structures related to fluctuating hydrodynamic conditions in floodplain deposits of the Beaufort Group near Beaufort West, Cape Province: Transactions of the Geological Society South Africa, v. 74, p. 111-113.

Ward, P.D., Montgomery, D.R., and Smith, R.M.H., 2000, Altered river morphology in South Africa related to the Permian-Triassic extinction: Science, v. 289, p. 1740-1743.

Ward, P.D., Botha, J., Buick, R., De Kock, M.O., Erwin, D.H., Garrison, G., Kirschvink, J., and Smith, R.H.M., 2005, Abrupt and gradual extinction among Late Permian land vertebrates in the Karoo Basin, South Africa: Science, v. 289, p. 1740-1743.

Wright, V.P., and Marriott, S.B., 2007, The dangers of taking mud for granted: Lessons from Lower Old Red Sandstone dryland systems of South Wales: Sedimentary Geology, v. 195, p. 91-100.

FIGURES

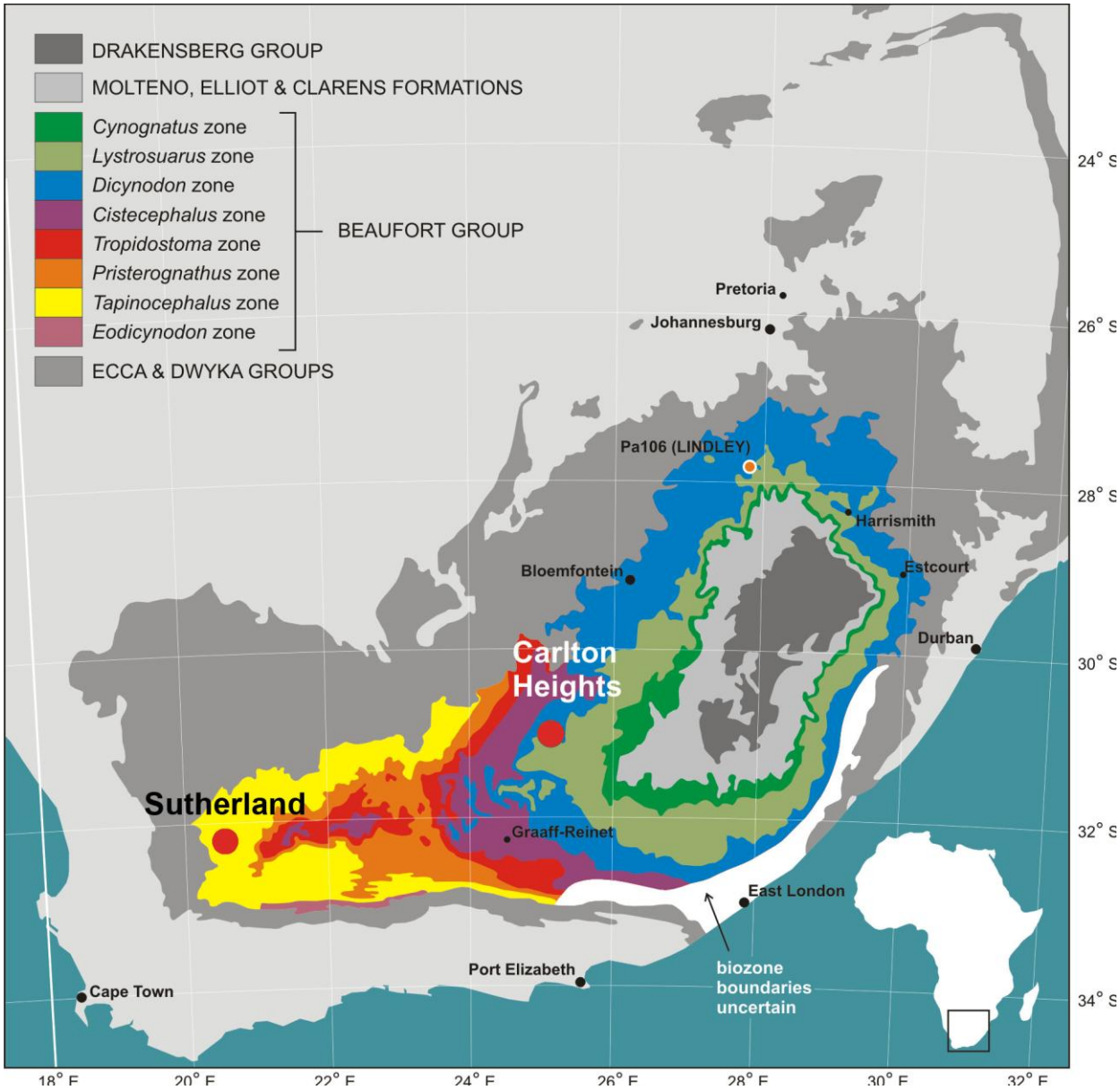

Figure 1: Biostratigraphic map of Karoo Basin deposits of southern Africa with sampling locations (Carlton Heights and Abrahamskraal Fm roadcut near Sutherland) marked by red circles. Inset: location of map within Africa.

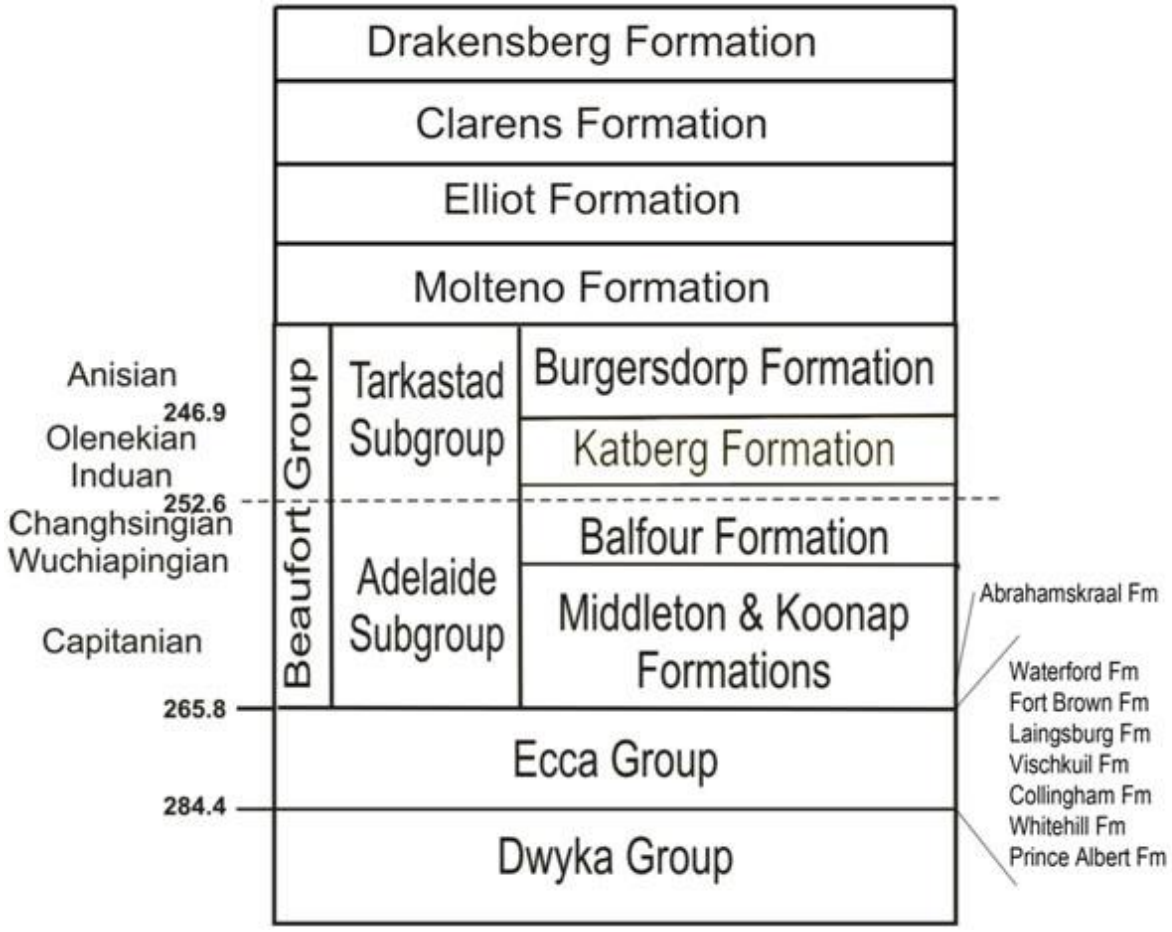

Figure 2: Generalized Karoo Basin stratigraphy. Dotted line indicates the PTB at 252.6 Ma after Mundil et al., 2004. Carlton Heights samples are from the lower Katberg Formation. Sutherland samples, from the Abrahamskraal Formation, are from the lowermost Adelaide Subgroup of the Beaufort Group.

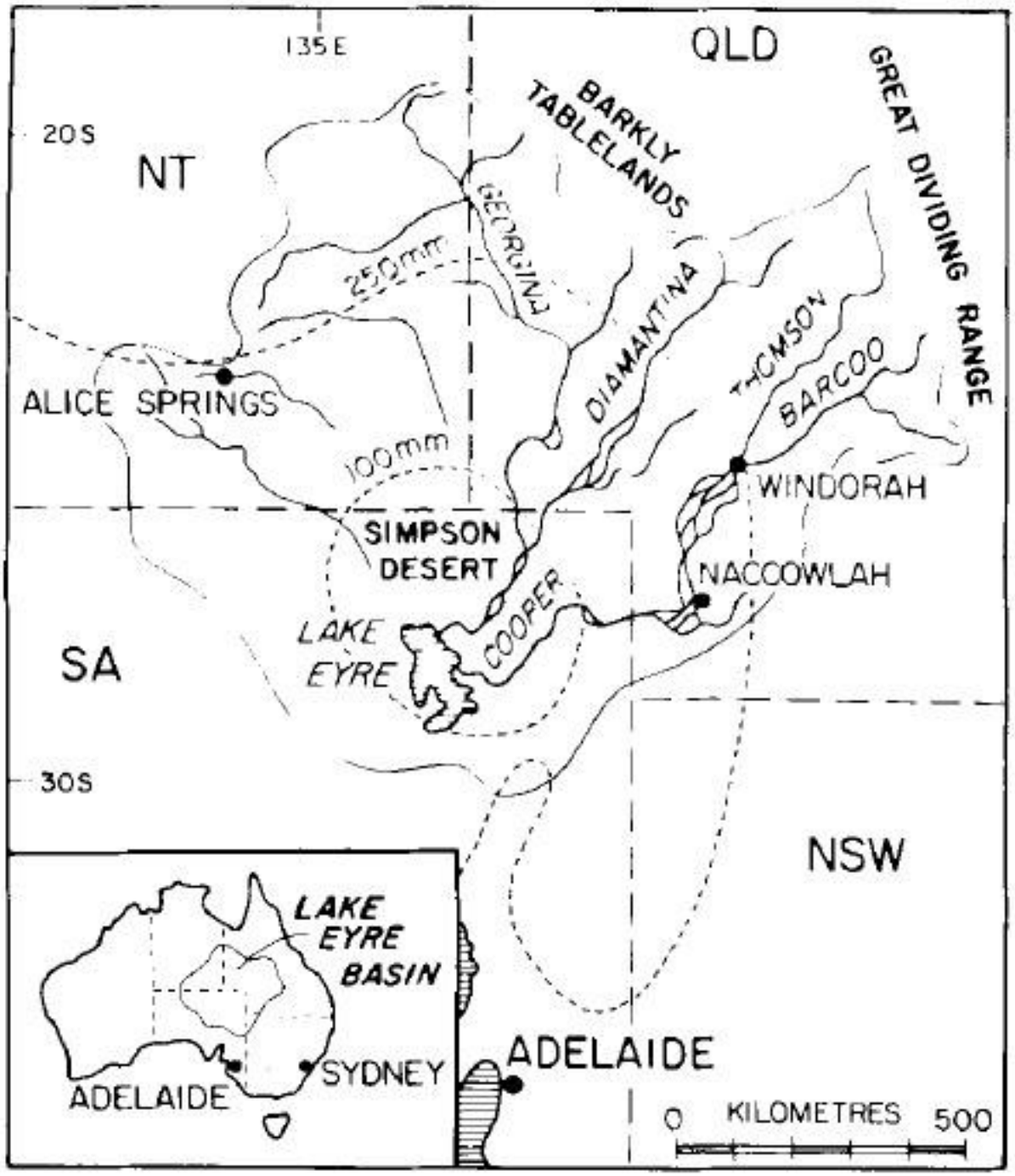

Figure 3: Map of the Lake Eyre Basin and its major rivers. Inset: location of basin within Australia. From Rust and Nanson, 1989.

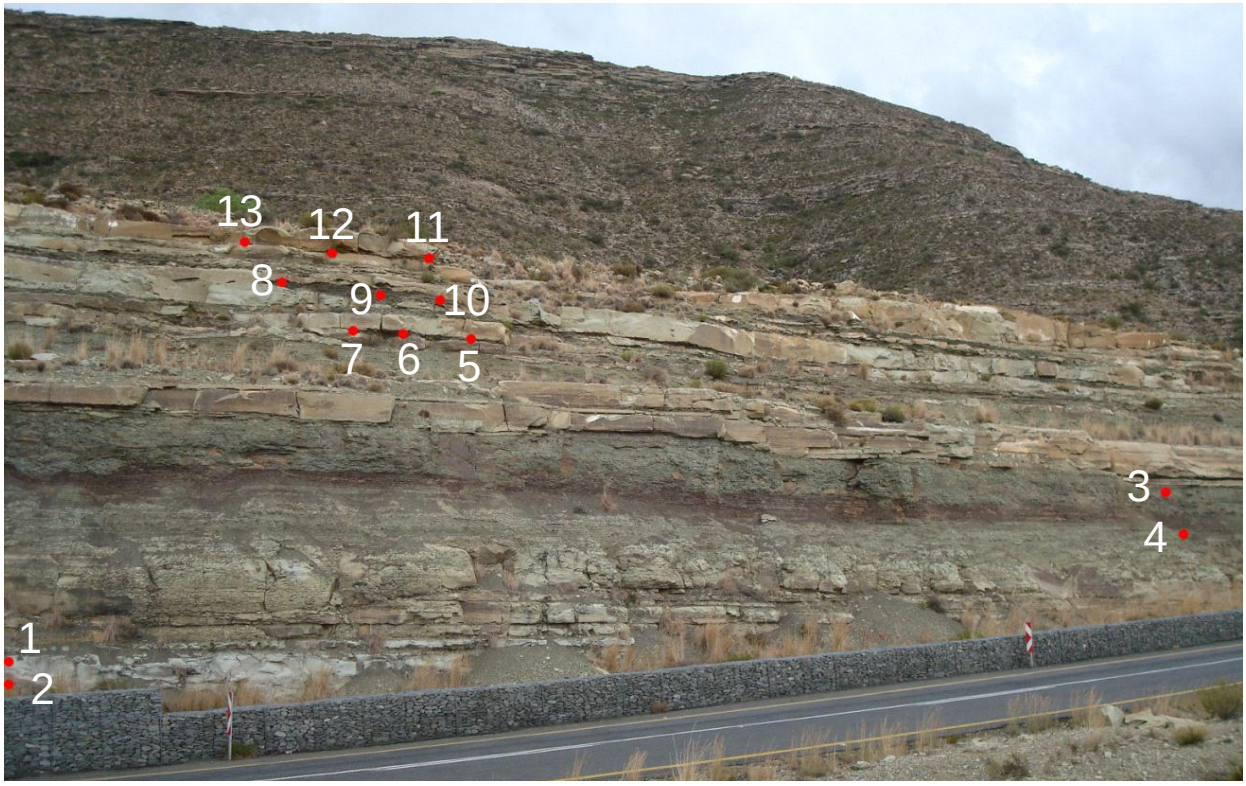

Figure 4: Carlton Heights, Eastern Cape Province, outcrop along the N-9 highway with sampling localities (numbers correspond to those on thin sections) marked. Sites 1-4 are from paleosols while 5-13 are sampled from siltstone lenses within three stories of channel bodies (SS3 of Pace et al., 2009).

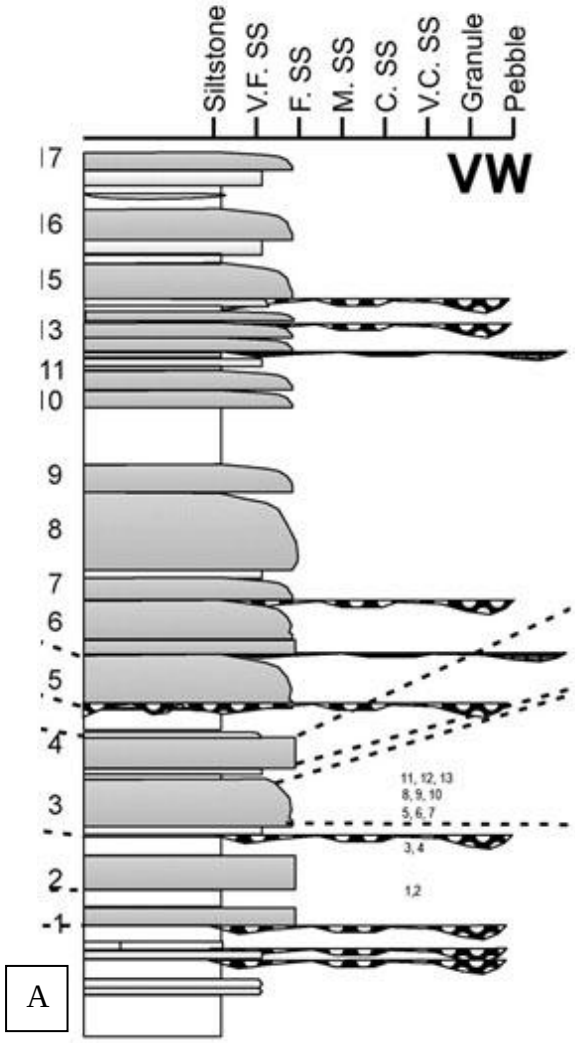

Figure 5: Location of samples in (A) generalized stratigraphic column of Carlton Heights (from Pace et al., 2009) and (B) outcrop photograph of Carlton Heights conglomeratic lag.

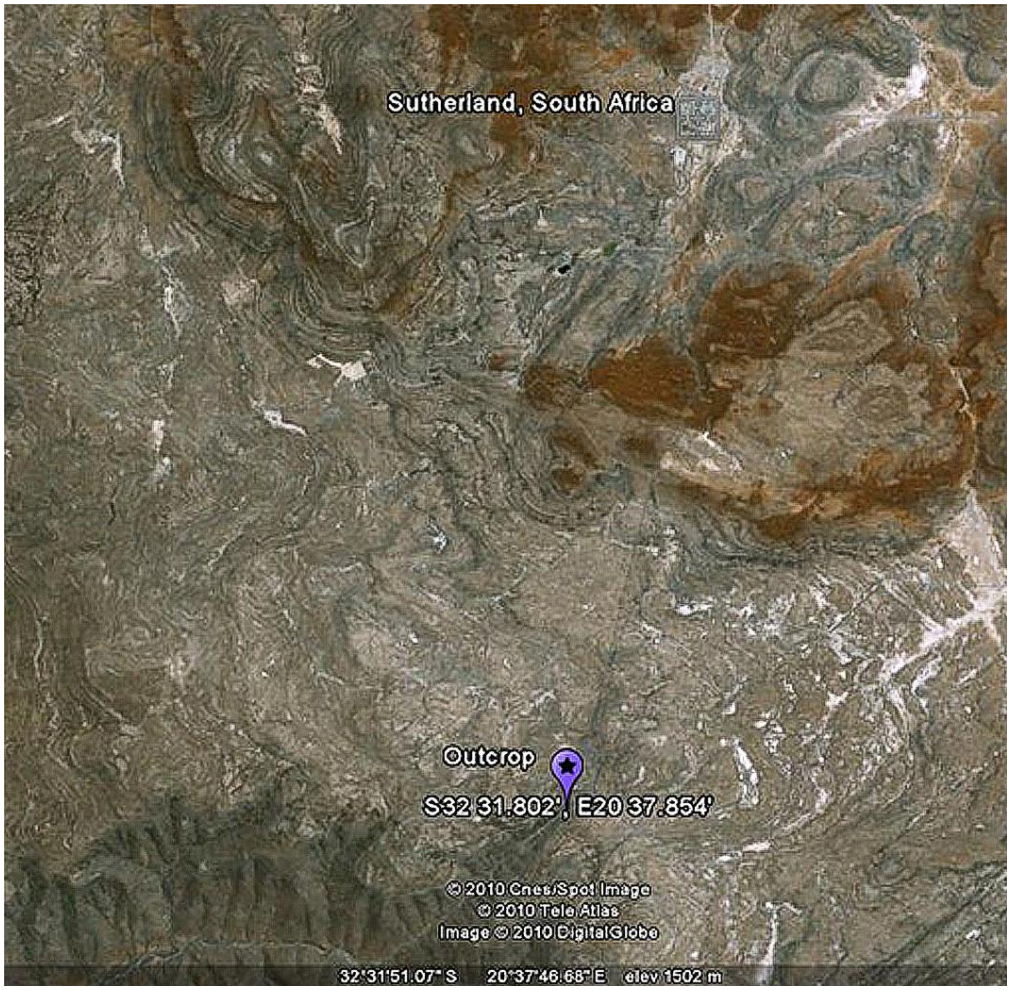

Figure 6: Satellite image from Google Earth showing location of Abrahamskraal outcrop (star bubble) in relation to Sutherland, South Africa. Outcrop is located at 32°S 31.802' 20°E 37.854' along the R354 highway in the Northern Cape Province.

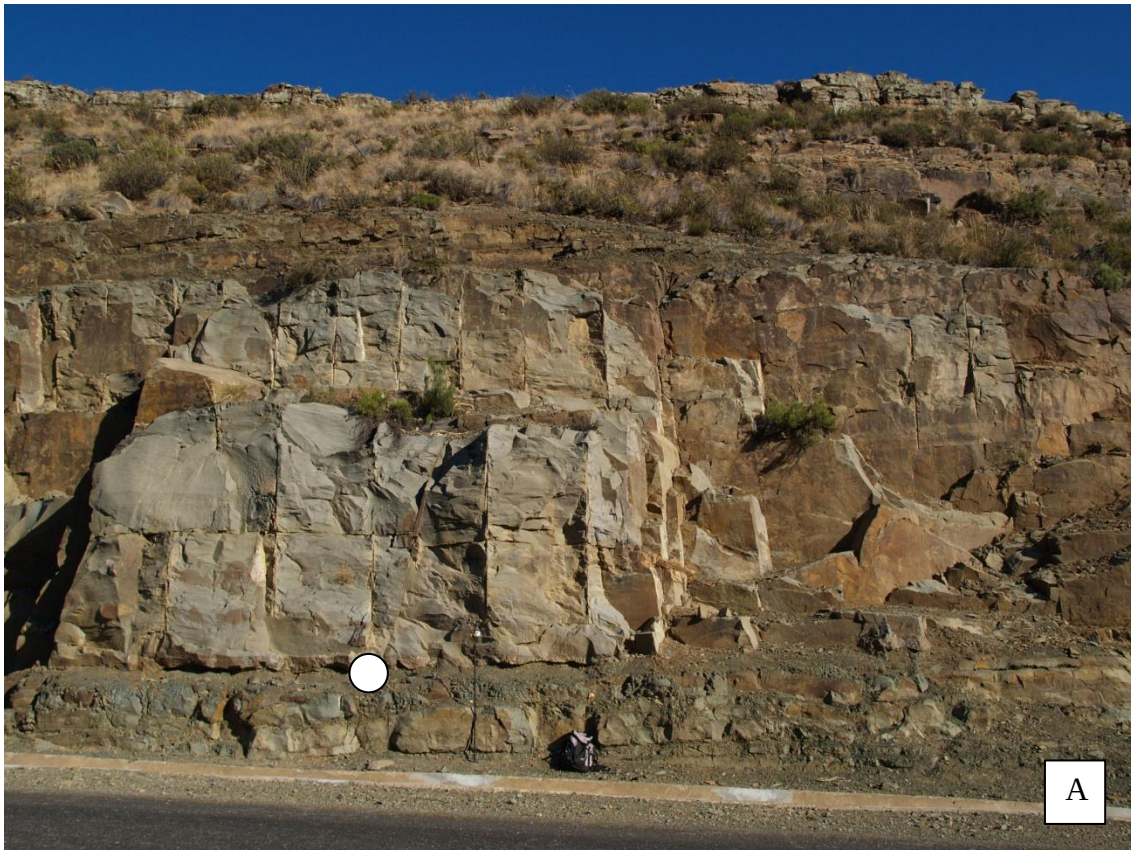

Figure 7: Abrahamskraal Formation roadcut near Sutherland. Sampling locality of conglomeratic lag is marked by circle in A. B shows outcrop photo of conglomeratic lag, scale is in decimeters.

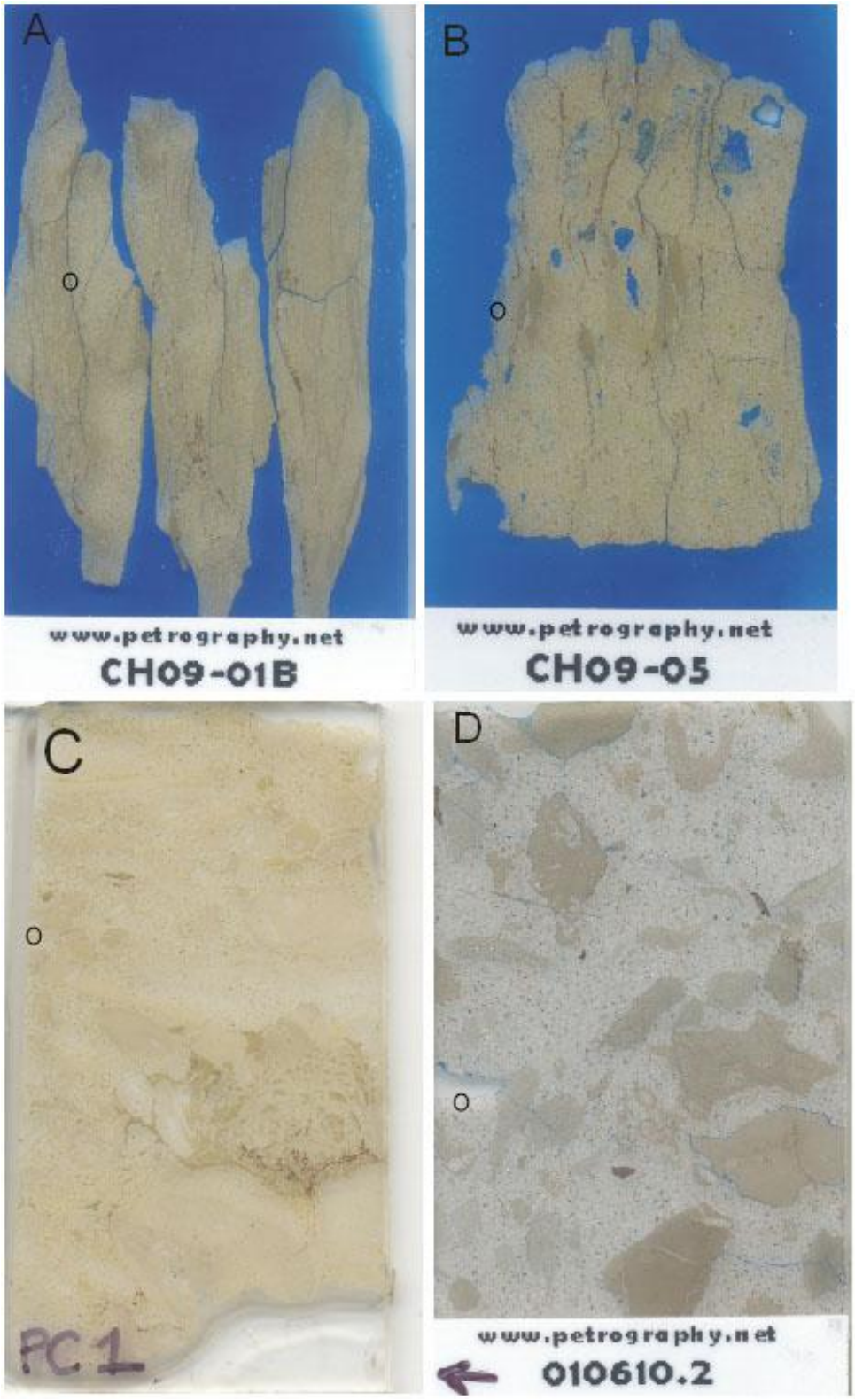

Figure 8: Thin section slides from samples of Carlton Heights paleosol (A), channel deposit (B), conglomeratic lag (C), and Sutherland conglomeratic lag (D) where arrow indicates stratigraphic up. Locations of BSE images on each slide are circled. Sample numbers (CH09-01B, CH09-05, PC1, 010610.2) correspond to collected samples. Each slide is 2.5 x 4.5 cm.

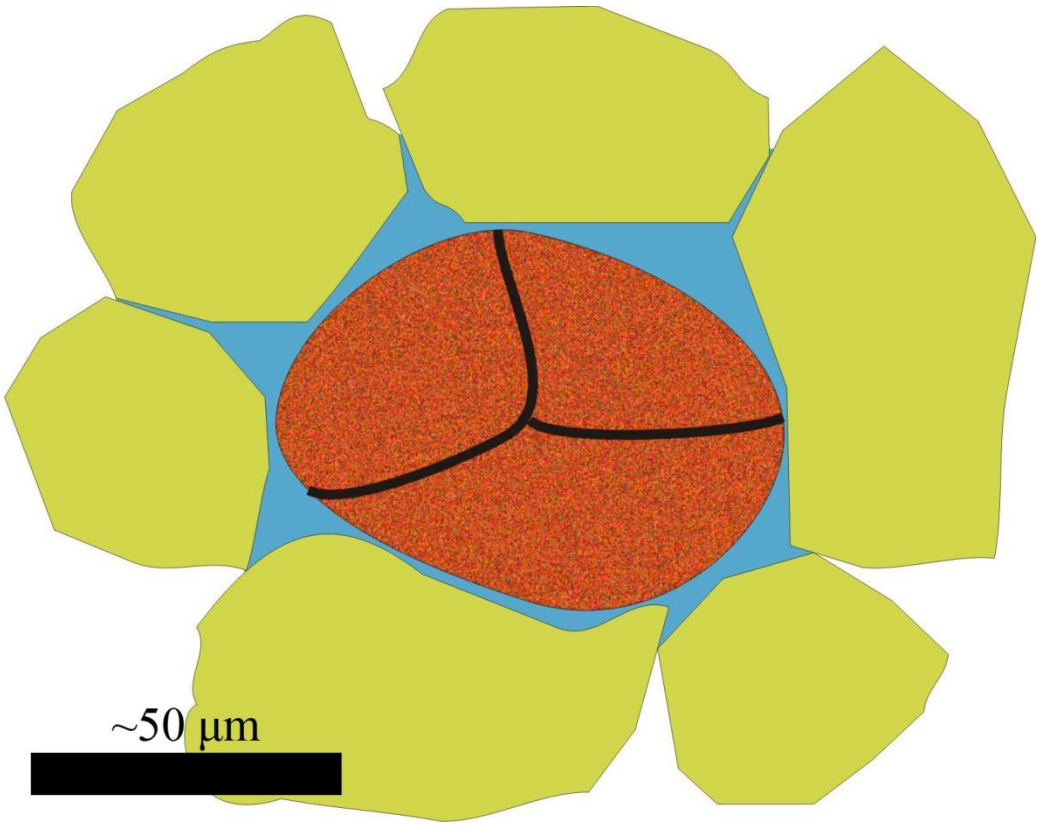

Figure 9: Idealized cartoon of pedogenic mud aggregate in thin section. The aggregate (brown, centered) is subangular and is clearly composed of three smaller mud clats that have been compacted together. The aggregate is surrounded by quartz grains (yellow) of approximately the same size. Pore space has been filled by blue epoxy which protects the shape of the aggregate.

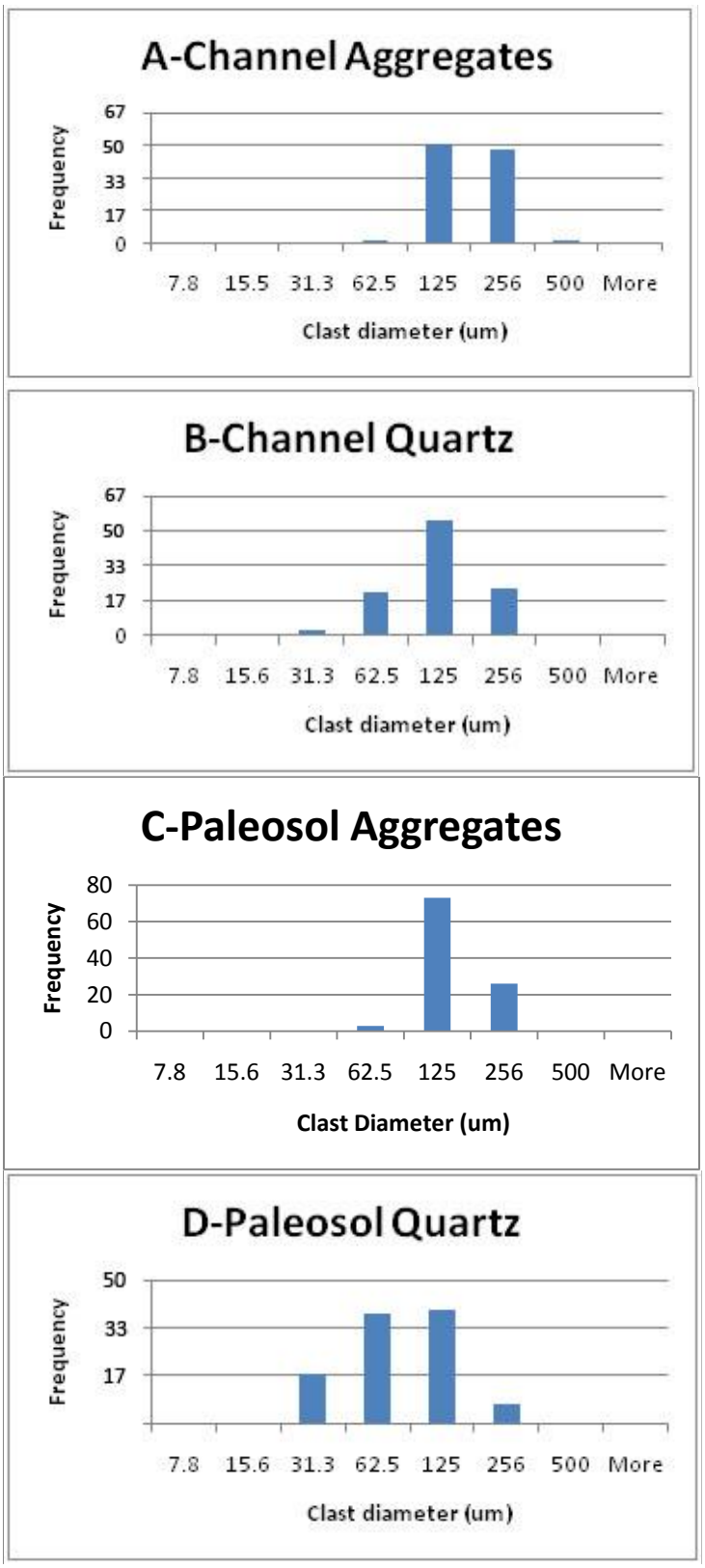

Figure 10: Histograms showing distribution of grain size of aggregates (A) and quartz (B) in Carlton Heights channels (samples CH09-01 to CH09-04) and of aggregates (C) and quartz (D) in Carlton Heights paleosols (samples CH09-05 to CH09-13).

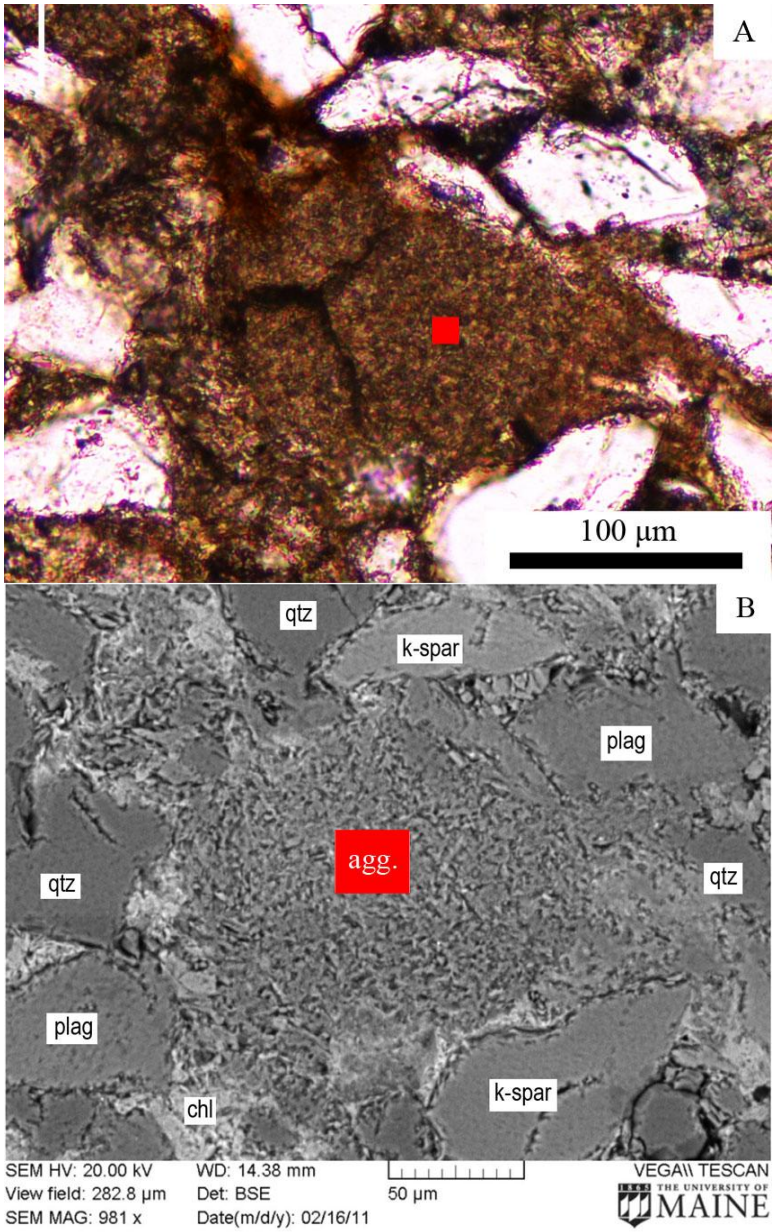

Figure 11: Photomicrograph (A) and backscatter electron image (B) of grains sampled from Carlton Heights paleosol (Sample CH09-01B). Scale bar on photomicrograph is 100 µm and is 50 µm on BSE image. Red square denotes site analyzed with EDS. Notation on backscatter image indicates mineralogy (qtz=quartz, kspar=potassium feldspar, plag=plagioclase, bt=biotite).

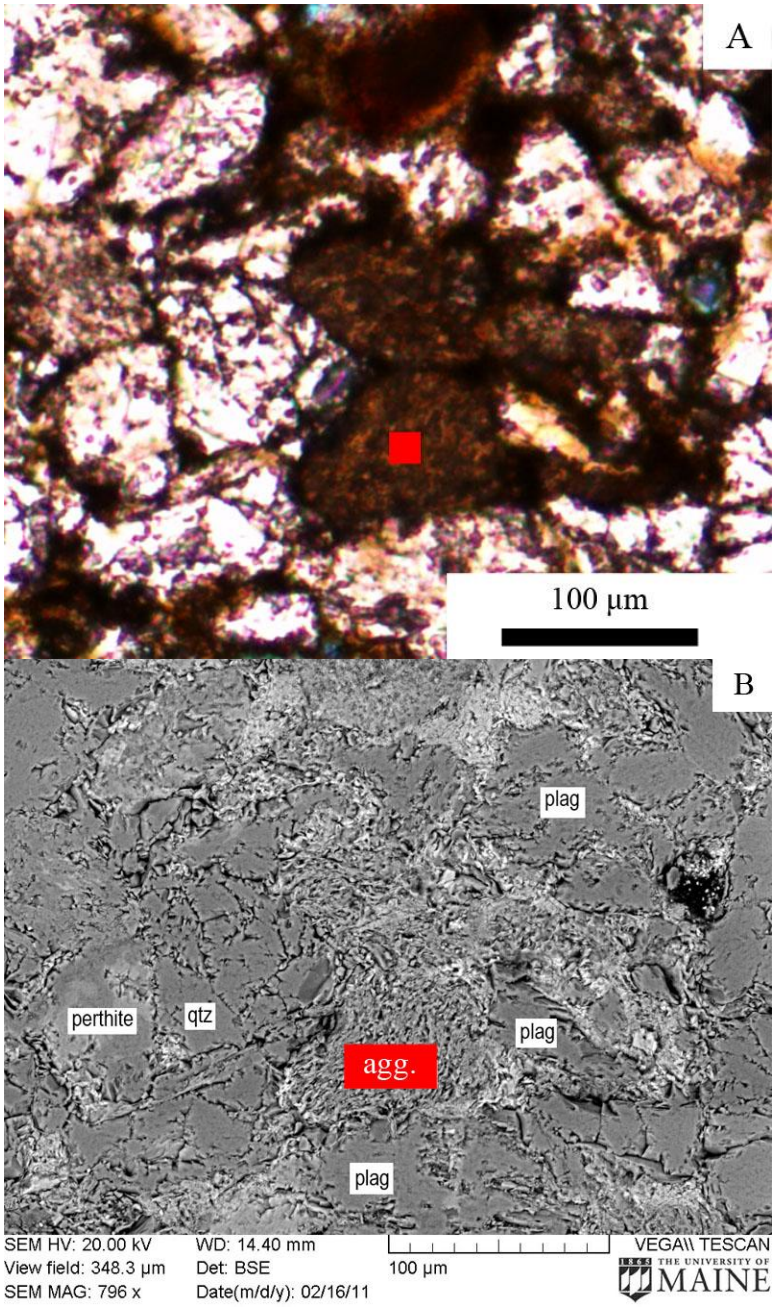

Figure 12: Photomicrograph (A) and backscatter electron image (B) of grains sampled from Carlton Heights channel (Sample CH09-05). Scale bar on both images is 100 µm. Red square denotes site analyzed with EDS. Notation on backscatter image indicates mineralogy (qtz=quartz, kspar=potassium feldspar, plag=plagioclase, bt=biotite).

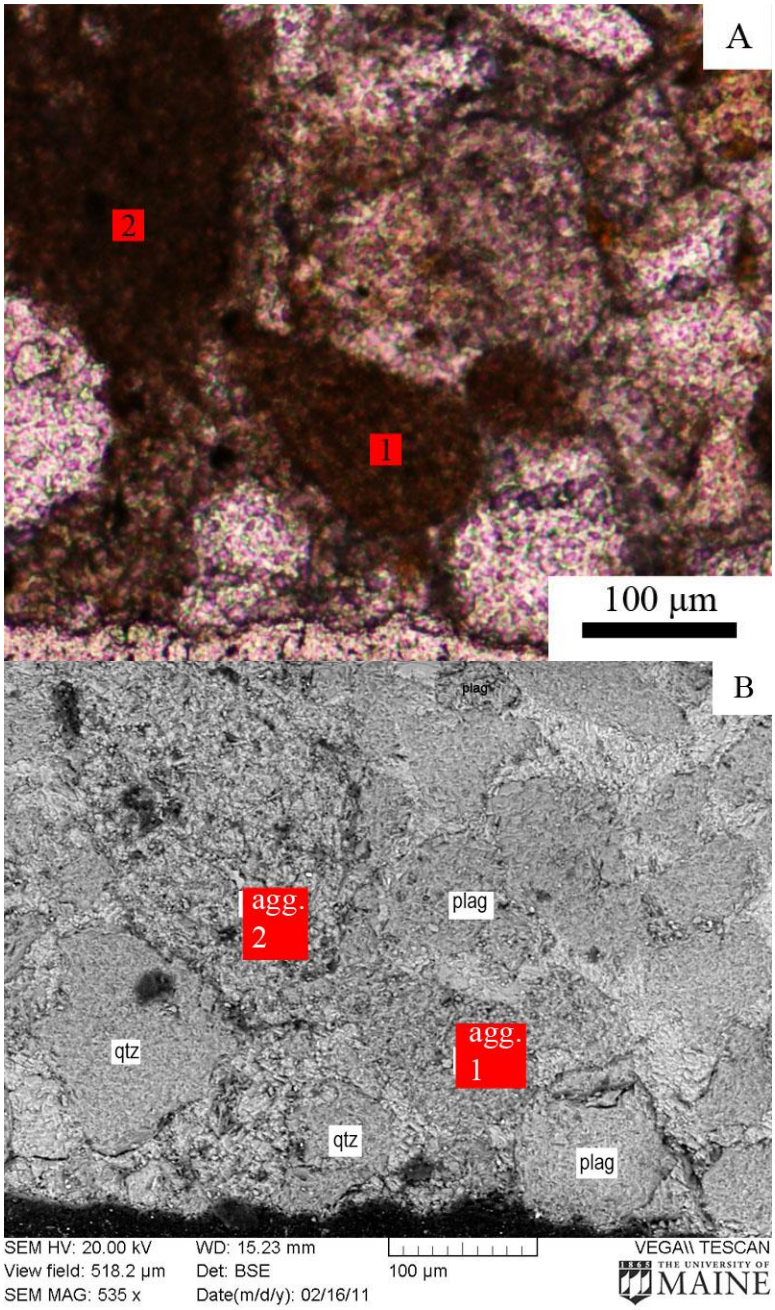

Figure 13: Photomicrograph (A) and backscatter electron image (B) of grains sampled from Carlton Heights conglomerate (Sample PC1). Scale bar on both images is 100 µm. Red square denotes site analyzed with EDS. Notation on backscatter image indicates mineralogy (qtz=quartz, kspar=potassium feldspar, plag=plagioclase, bt=biotite).

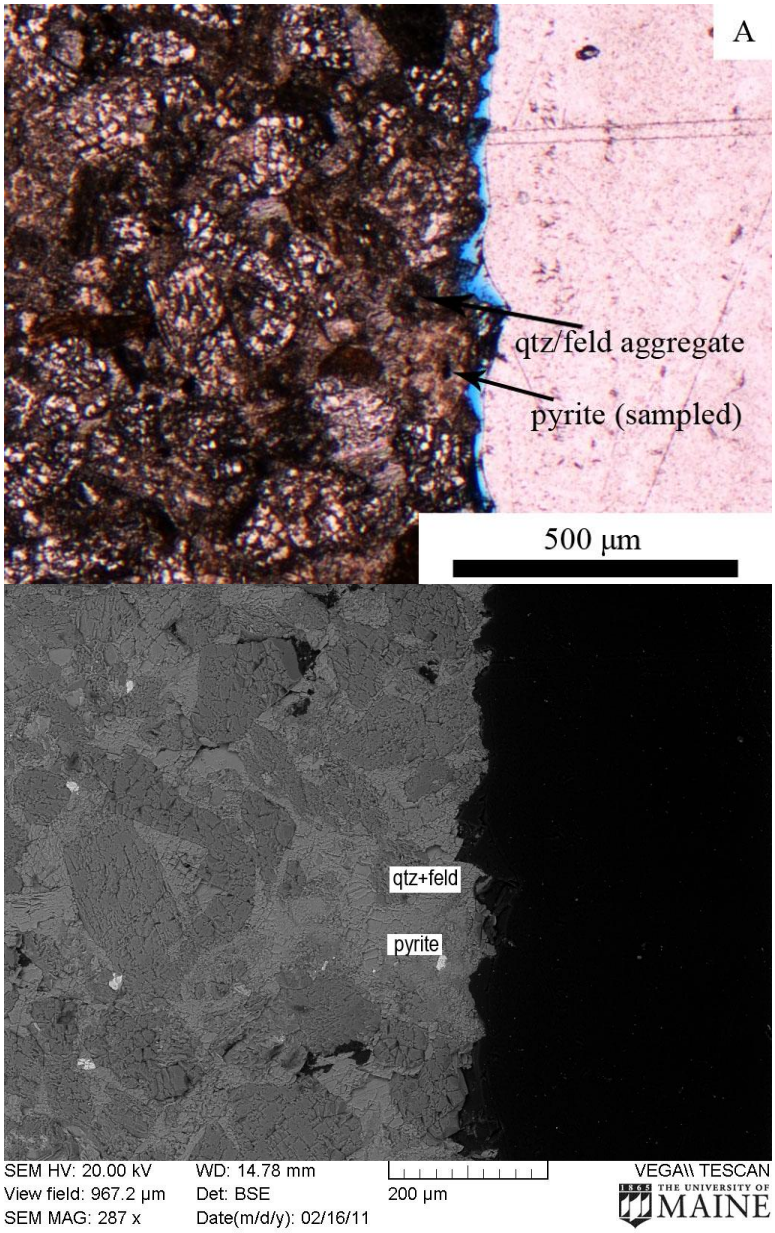

Figure 14: Photomicrograph (A) and backscatter electron image (B) of grains sampled from Abrahamskraal conglomerate (Sample 010610.2). Scale bar on photomicrograph is 500 µm and is 200 µm on BSE image. Pyrite grain indicated was analyzed with EDS. Notation on backscatter image indicates mineralogy (qtz=quartz, feld=feldspar).

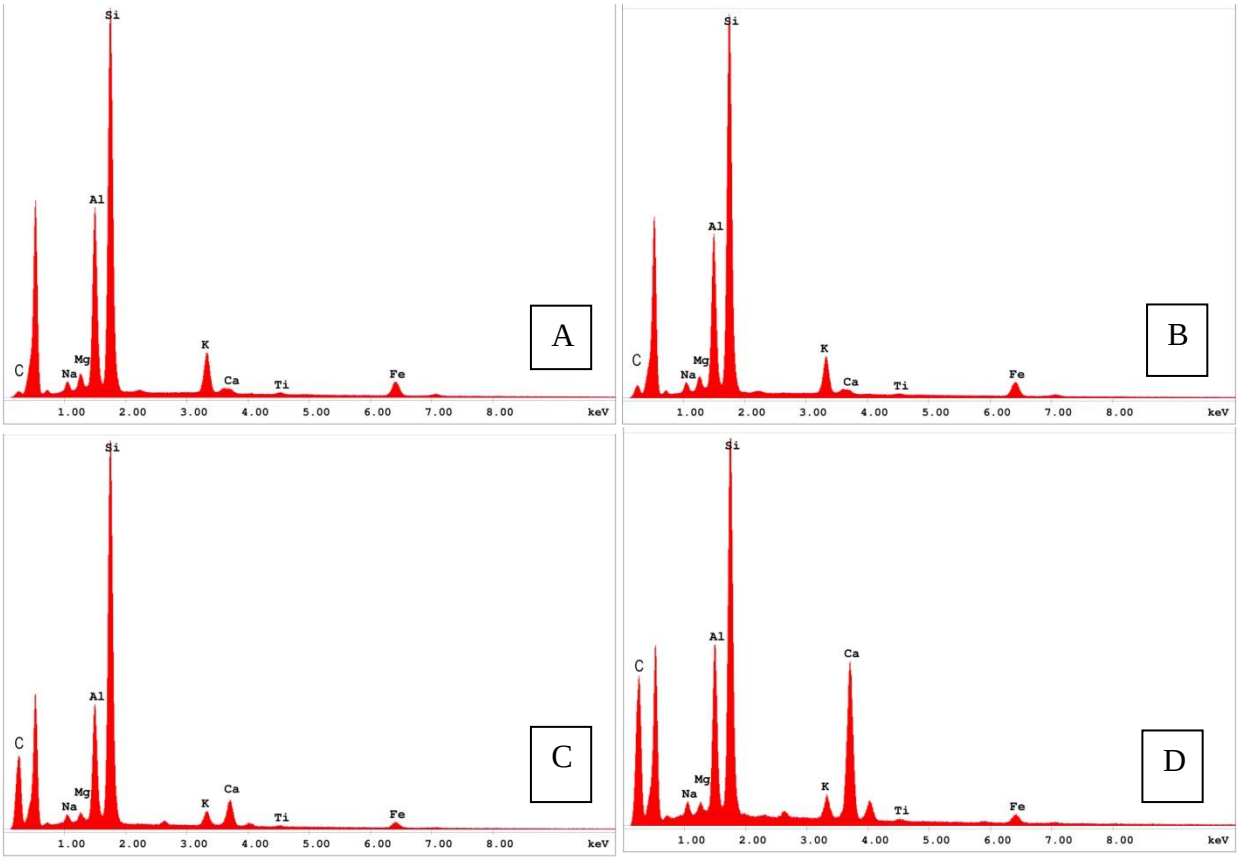

Figure 15: EDS spectra showing chemical distributions from aggregates in Carlton Heights paleosol (A- sample CH09-01B), channel (B- sample CH09-05), and conglomerate (C- 1, D- 2- Sample PC-1).

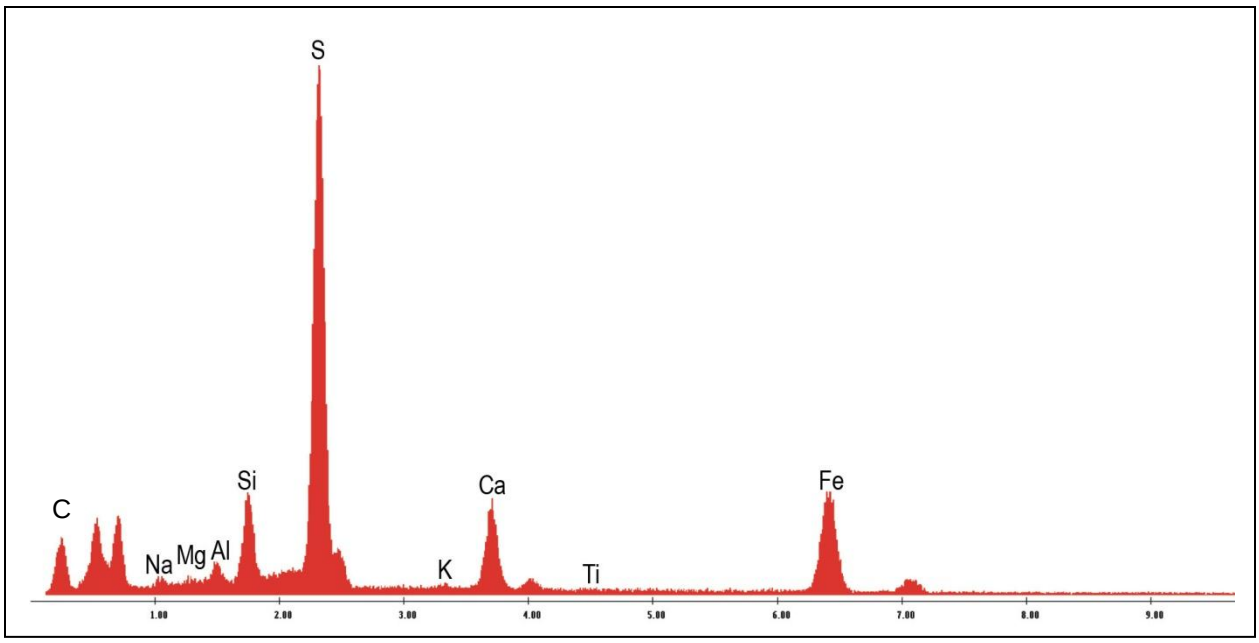

Figure 16: EDS spectrum from Sutherland sample (010610.2). Sample was determined to be pyrite rich (FeS_2).

APPENDICES

	Channel size (um)		Paleosol size (um)	
	Aggregates	Quartz	Aggregates	Quartz
	110.92	45.31	172.43	116.89
	138.31	87.24	165.12	99.61
	99.11	74.47	91.8	111.91
	141.92	45.91	146.09	64.5
	198.95	57.62	101.59	101.41
	150.19	61.54	80.95	98.99
	107.07	99.67	94.71	182.9
	140.58	72.77	65.31	99
	127.56	72.58	111.72	109.89
	138.16	101.1	95.63	167.62
	121.57	145.29	133.56	61.39
	154.99	84.87	85.13	128.87
	115.43	207.37	106.4	117.33
	165.65	95.97	93.86	165.42
	150.08	74.75	121.54	63.25
	94.59	86.34	83.35	61.06
	109.52	182.08	149.99	78.77
	113.74	219.39	76.1	65.6
	130.57	84.44	108.07	180.97
	150.16	176.16	57.72	100.99
	127.04	128.73	62.6	87.08
	111.24	154.88	151.9	66.72
	126.35	131.53	112.28	47.74
	163.52	150.17	135.12	42.69
	59.59	98.73	162.47	115.39
	75.38	96.74	100.7	114.52
	110.4	154.37	142.39	100.67
	110.68	39.9	118.64	91.85
	173.07	81.27	91.97	63.11
	270.12	187.31	228.09	55.46
	118.92	215.34	78.71	120.95
	167.39	127.03	102.3	88.53
	73.51	85.15	78.62	99.75
	181.9	110.19	137.88	124.55
	98.53	325.14	102.77	124.19
	105.13	114.68	66.27	114.27
	152.41	156.9	85.51	63.34
	130.41	54.09	117.46	234.61
	101.27	54.36	86.33	85.33

	Channel size (um)		Paleosol size (um)	
	Aggregates	Quartz	Aggregates	Quartz
	97.3	55.47	134.59	103.55
	99.7	136.65	109.75	98.68
	111.01	35.47	133.07	110.35
	97.76	150	61.1	95.45
	120.47	89.58	81.49	148.38
	199	82.97	116.33	59.58
	92.68	118.55	71.63	82.12
	110.72	136.59	69.91	93.11
	145.81	98.76	125.55	96.59
	169.47	117.89	113.8	211.58
	136.82	74.08	93.39	42.54
	212.73	121.66	62.7	124.03
	82.6	204.27	85.3	162.67
	73.81	95.76	114.72	128.51
	104.71	166.27	143.73	135.61
	164.99	74.37	124.34	217.35
	194.92	121.03	129.08	121.69
	98.97	49.62	121.8	121.69
	167.78	88.25	129.08	167.92
	130.45	113.71	100.12	107.93
	137.44	76.66	155.73	54.97
	164.53	114.39	114.86	77.3
	154.24	160.65	82.5	52
	127.24	125.16	125.61	50.12
	149.06	119.79	166.68	88.54
	123.59	50.65	93.86	87.96
	126.38	42.93	103.19	216.5
	168.64	92.47	117.62	80.01
	127.83	57.03	81.12	87.25
	131.31	71.83	70.22	82.94
	171.74	85.95	81.98	74.06
	99.95	110.82	95.71	106.01
	109.53	110.46	102.77	57.57
	151.78	106.28	130.45	84.2
	103.59	71.21	84.7	110.09
	150.77	100.13	119.46	27.74
	108.06	67.78	127.82	38.87
	127.99	105.18	73.63	106.35
	85.59	75.09	63.34	67.48

	Channel size (um)		Paleosol size (um)	
	Aggregates	Quartz	Aggregates	Quartz
	88.64	120.06	74.77	46.84
	99.93	90.63	86.71	79.91
	111.14	65.98	89.81	72.6
	73.92	148.88	81.73	38.76
	118.6	77.44	46.57	35.9
	103.15	81.64	81.73	63.74
	100.88	54.07	106.57	81.63
	44.16	136.65	149.07	75.14
	93.9	72.89	88.04	59.63
	213.42	63.53	88.94	194.43
	74.05	73.25	98.75	137.28
	83.49	101.58	114.28	65.82
	129.43	81.13	87.47	45.27
	81.37	81.13	118.25	89.81
	133.62	41.98	70	57.27
	84.37	41.89	83.69	46.74
	99.55	64.37	103.22	42.94
	147.14	48.35	65.46	29.96
	93.22	53.82	115.2	220.71
	201.46	90.63	175.37	89.49
	136.51	71.31	141.33	108.53
	158.12	80.22	175.76	69.91
	114.69	77.69	119.03	37.14
	98.66	160.58	118.85	46.65
	110.66	107.09		16.11
	120.8	59.7		28.72
	96.31	117.58		40.2
	56.64	71.35		26.57
	128.33	94.95		23.29
	116.88	73.02		24.33
	109.17	113.45		47.87
	159.41	87.03		29.45
	155.86	83.78		36.42
	149.87	64.92		25.33
	162.26	48.29		32.06
	72.1	44.02		49.17
	116.88	53.32		77.07
	102.87	33.38		31.1
	65.34	160.26		27.74

	Channel size (um)		Paleosol size (um)	
	Aggregates	Quartz	Aggregates	Quartz
	132.42	54.21		30.43
	97.06	43.58		66.64
	84.03	77.61		62.5
	121.64	55.47		32
	121.62	67.47		21.54
	111.13	87.33		34.9
	131.2	103.95		41.42
	109.62	176.99		35.23
	127.5	237.84		23.29
	92.69	69.98		21.33
	92.39	107.91		35
	97.32	34.45		32.11
	87.68	122.2		28.72
	109.94	58.87		48.53
	97.14	86.36		46.44
	71.11	116.25		32.55
	94.29	94.59		18.14
	130.11	27.06		42.75
	97.32	33.46		59.63
	124.85	33.46		24.04
	160.81	121.91		21.87
	109.79	58.5		64.8
	80.27	64.54		66.72
	227.2	54.12		23.63
	89.12	134.33		29.33
	117.33	25.68		69.91
	166.37	27.2		28.63
	94.69	70.32		26.67
	93.45	31.2		23.29
	71.99	32.91		34.59
	124.07	204.38		61.98
	116.61	68.29		67
	98.95	109.2		48.02
	89.34	111.02		76.93
	122.44	129		78.68
	101.53	57.01		77.31
	113.64	28.67		91.85
	148.42	37.86		68.99
	174.12	46.54		107.07

	Channel size (um)		Paleosol size (um)	
	Aggregates	Quartz	Aggregates	Quartz
	92.69	55.12		77.07
	127.44	115.38		120.8
	89.96	245.05		100.92
	135.21	91.81		47.29
	137.64	31.63		64.22
	139.4	40.54		41.16
	119.75	116.44		38.94
	150.25	68.92		75.25
	125.07	71.63		36.88
	90.23	93.52		55.46
	142.03	16.44		45.88
	104.32	44.12		74.86
	89.37	43.24		81.1
	105.6	25.71		97.65
	216.11	43.58		66.57
	138.33	48.23		63.74
	145.76	45.89		57.89
	161.59	191.58		69.77
	209.32	184.46		81.51
	129.16	157.74		59.4
	59.59	136.51		64.51
	93.69	326.8		81.33
	57.49	177.08		63.39
	97.76	153		74.96
	108.11	71.72		70.36
	100.44	65.09		123.8
	95.25	73.73		74.21
	135.51	94.6		77.52
	140.55	71.35		72.17
	109.46	101.28		58.58
	164.92	163.3		62.15
	109.74	103.14		74.06
	129.9	82.3		73.64
	159.75	156.71		66.21
	225.7	86.5		82.84
	127.17	110.82		69.6
	145.93	168.46		86.67
	150.08	80.22		29.12
	140.22	58.67		74.63

	Channel size (um)		Paleosol size (um)	
	Aggregates	Quartz	Aggregates	Quartz
	199.29	47.61		51.78
	133.07	105.86		116.95
	107.29	162.72		41.07
	109.19	104.76		61.17
	125.37	212.06		57.89
	108.31	125.76		71.62
	166.5	111.21		50.6
	156.23	152.08		63.68
	106.1	127.61		69.6
	123.33	161.17		46.1
	111.53	77.12		20.88
	96.17	46.22		30.15
	203.57	101.31		46.04
	86.19	72.99		50.6
	114.86	162.3		65.73
	92.21	113.01		31.14
	125.2	108.18		57.01
	124.74	184.21		55.44
	113.8	149.27		35.36
	108.07	150.7		38.41
	107.78	99.42		56.6
	152.28	109.67		56.45
	138.47	97.63		46.44
	102.77	53.24		61.54
	124.43	81.18		43.33
	192.66	46.91		108.19
	95.17	42.41		80.14
	229.77	97.54		50.89
	167.3	56.77		32.71
	163.95	117.34		51.72
	156.52	90.85		45.97
	141.44	164.33		35.47
	136.5	92.37		45.41
	208.85	74.53		117.32
	82.52	107.61		27.16
	171.77	137.98		66.44
	117.15	91.83		73.55
	96.54	63.79		63.87
	123.99	76.75		44.76

	Channel size (um)		Paleosol size (um)	
	Aggregates	Quartz	Aggregates	Quartz
	104.39	193.09		71.67
	153.89	79.74		32.68
	88.65	85.23		33.81
	143.37	77.39		36.49
	138.97	119.41		25.71
	133.49	63.1		35.37
	125.24	109.99		46.54
	141.63	65.22		60.74
	108.06	61.23		42.09
	146.4	114.86		38.22
	161.21	98.2		40.56
	72.94	50.07		34.61
	122.55	111.97		48.97
	146.88	52.7		28.51
	140.55	170.51		66.67
	70.14	120.09		32.71
	89.8	118		67.22
	116.88	138.08		114.98
	169.19	137.73		21.66
	150.39	126.68		41.63
	138.72	59.52		57.73
	85.83	108.19		58.87
	124.8	67.58		28.89
	168.69	76.94		52.2
	124.5	70.28		22.65
	153.09	113.14		19.11
	120.32	196.99		31.55
	153.53	88.68		23.6
	128.43	54.88		36.88
	112.22	159.83		33.81
	132.02	155.05		39.74
	135.02	44.27		36.49
	160.81	88.46		30.37
	153.88	132.25		27.83
	122.79	61.42		30.87
	76.65	118.95		37.86
	156.12	100.45		31.08
	129.88	91.93		46.54
	84.87	66.55		56.82

	Channel size (um)		Paleosol size (um)	
	Aggregates	Quartz	Aggregates	Quartz
	156.25	116.41		32.12
	93.36	81.81		19.68
	137.45	129.87		21.15
	78.7	128.75		27.16
	108.71	58.62		47.61
	117.72	67.78		23.01
	86.18	122.44		25.71
	215.21	137.86		46.66
	161.41	100.37		24.36
	132.64	74.53		31.11
	68.83	55.42		26.55
	86.5	58.87		31.08
	149.28	142		41.45
	134.4	89.9		28.38
	103.91	106.76		35.14
	152.64	104.72		46.12
	145.38	72.97		37.84
	149.33	72.43		35.16
	158.56	110.88		55.47
	115.04	127.89		21.62
	172.46	75.78		35.47
	90.67	100.23		47.2
	116.11	97.54		32.54
	143.77	63.04		81.09
	149.71	62.29		133.59
	126.51	101.75		146.2
	143.34	159.83		131.1
		116.64		120.33
		55.72		53.24
		107.6		57.84
		143.4		
Average	125.96	98.33457	106.827549	66.59208
Max	270.12	326.8	228.09	234.61
Min	44.16	16.44	46.57	16.11

Appendix 1: Size measurements of channel aggregates (from samples CH09-05 – CH09-13), channel quartz, paleosol aggregates (from samples CH09-01 – CH09-04, and paleosol quartz as well as average, maximum, and minimum size for each category.

CH09-01B Paleosol						
Element	Wt %	Mol %	K-Ratio	Z	A	F
Na2O	1.53	1.68	0.0042	0.9652	0.3861	1.0044
MgO	2.14	3.62	0.0068	0.9830	0.5324	1.0086
Al2O3	23.91	15.99	0.0804	0.9489	0.6630	1.0100
SiO2	59.41	67.41	0.1788	0.9720	0.6618	1.0008
K2O	5.29	3.83	0.0354	0.9111	0.8838	1.0026
CaO	0.79	0.96	0.0048	0.9294	0.9023	1.0029
TiO2	0.75	0.64	0.0036	0.8442	0.9537	1.0061
FeO	6.18	5.87	0.0398	0.8325	0.9952	1.0000
Total	100.00	100.00				

CH09-05 Channel						
Element	Wt %	Mol %	K-Ratio	Z	A	F
Na2O	1.65	1.80	0.0046	0.9649	0.3865	1.0044
MgO	2.12	3.54	0.0067	0.9827	0.5319	1.0085
Al2O3	21.84	14.46	0.0734	0.9486	0.6626	1.0105
SiO2	61.63	69.22	0.1881	0.9717	0.6713	1.0008
K2O	5.05	3.62	0.0338	0.9109	0.8838	1.0024
CaO	0.66	0.79	0.0039	0.9291	0.9033	1.0028
TiO2	0.46	0.39	0.0022	0.8439	0.9545	1.0066
FeO	6.60	6.20	0.0425	0.8323	0.9957	1.0000
Total	100.00	100.00				

PC1- Congl. Sample 1						
Element	Wt %	Mol %	K-Ratio	Z	A	F
Na2O	1.41	1.49	0.0041	0.9599	0.4024	1.0046
MgO	1.28	2.08	0.0042	0.9777	0.5511	1.0091
Al2O3	18.19	11.64	0.0631	0.9437	0.6861	1.0123
SiO2	67.94	73.78	0.2169	0.9666	0.7059	1.0008
K2O	2.25	1.56	0.0151	0.9061	0.8853	1.0066
CaO	5.46	6.35	0.0330	0.9242	0.9145	1.0015
TiO2	0.52	0.43	0.0025	0.8394	0.9506	1.0028
FeO	2.94	2.67	0.0188	0.8277	0.9940	1.0000
Total	100.00	100.00				

PC1- Congl. Sample 2						
Element	Wt %	Mol %	K-Ratio	Z	A	F

Na2O	1.89	1.97	0.0051	0.9697	0.3762	1.0037
MgO	1.35	2.17	0.0042	0.9876	0.5195	1.0074
Al2O3	19.30	12.27	0.0645	0.9543	0.6560	1.0092
SiO2	48.83	52.66	0.1520	0.9766	0.6803	1.0022
K2O	2.35	1.62	0.0166	0.9156	0.9054	1.0261
CaO	22.32	25.79	0.1387	0.9340	0.9294	1.0016
TiO2	0.69	0.56	0.0032	0.8485	0.9237	1.0025
FeO	3.29	2.96	0.0210	0.8371	0.9823	
Total	100.00	100.00				

Appendix 2- Quantitative analyses of oxide composition from SEM analysis of aggregates in Carlton Heights paleosol (sample 01B), channel (sample 05), and conglomerate (PC1).